ELSEVIER

Journal of Nuclear Materials 273 (1999) 1–26

journal of nuclear materials

www.elsevier.nl/locate/jnucmat

Review

Hydrogen isotope retention in beryllium for tokamak plasma-facing applications

R.A. Anderl [a], R.A. Causey [b], J.W. Davis [d], R.P. Doerner [c], G. Federici [e], A.A. Haasz [d], G.R. Longhurst [a,*], W.R. Wampler [b], K.L. Wilson [b]

[a] *Lockheed Martin Idaho Technologies Company, Idaho National Engineering and Environmental Laboratory, P.O. Box 1625, Idaho Falls ID 83415-3860, USA*

[b] *Sandia National Laboratories, Livermore, CA, Albuquerque, NM, USA*

[c] *University of California, San Diego, La Jolla, CA, USA*

[d] *Institute for Aerospace Studies, University of Toronto, Toronto, Canada*

[e] *ITER JWS Garching Co-center, Garching, Germany*

Received 17 August 1998; accepted 29 December 1998

Abstract

Beryllium has been used as a plasma-facing material to effect substantial improvements in plasma performance in the Joint European Torus (JET), and it is planned as a plasma-facing material for the first wall (FW) and other components of the International Thermonuclear Experimental Reactor (ITER). The interaction of hydrogenic ions, and charge-exchange neutral atoms from plasmas, with beryllium has been studied in recent years with widely varying interpretations of results. In this paper we review experimental data regarding hydrogenic atom inventories in experiments pertinent to tokamak applications and show that with some very plausible assumptions, the experimental data appear to exhibit rather predictable trends. A phenomenon observed in high ion-flux experiments is the saturation of the beryllium surface such that inventories of implanted particles become insensitive to increased flux and to continued implantation fluence. Methods for modeling retention and release of implanted hydrogen in beryllium are reviewed and an adaptation is suggested for modeling the saturation effects. The TMAP4 code used with these modifications has succeeded in simulating experimental data taken under saturation conditions where codes without this feature have not. That implementation also works well under more routine conditions where the conventional recombination-limited release model is applicable. Calculations of tritium inventory and permeation in the ITER FW during the basic performance phase (BPP) using both the conventional recombination model and the saturation effects assumptions show a difference of several orders of magnitude in both inventory and permeation rate to the coolant.

PACS: 52.40.Hf; 61.80.Jh; 68.55.Ln; 66.30.Jt

1. Introduction

Beryllium has for several years been considered a primary candidate for plasma-facing components (PFCs) in tokamaks because of its low atomic number and excellent oxygen gettering capabilities [1]. Both of these features result in a lower Z_{eff} for the plasma. After incorporating beryllium as a FW material in the Joint European Torus (JET), first by evaporating beryllium over other internal surfaces and then by using beryllium tiles in the vessel bottom facing the X-point, an improvement in plasma performance was seen as manifested by increases in deuterium ion density, deuterium ion temperature, and energy confinement time [2,3]. The addition of beryllium also resulted in a more than doubling of the fueling rate requirement as well as a marked increase in the post-shot gas release [4].

* Corresponding author. Tel.: +1-208 526 9950; fax: +1-208 526 2930; e-mail: gxl@inel.gov.

0022-3115/99/$ – see front matter
PII: S0022-3115(99)00022-7

This paper concerns one key issue in the evaluation of materials for PFC applications, namely, tritium uptake, retention, and permeation. Quantitative predictions for these processes are important because they affect safety assessments, fuel economy, and tokamak plasma operational performance. In general, the factors that influence uptake and retention include specific material type, temperature, defect microstructure, surface properties, hydrogen solubility, diffusivity and surface recombination [5,6].

Our specific purpose is to establish the scientific framework for a realistic prediction of tritium uptake and retention in Be that might be used as a PFC material in next-step tokamaks like ITER. This task is accomplished in two ways: (1) by critically reviewing the experimental data base from the perspective of ITER-relevant conditions such as particle flux, energy, and fluence and (2) by presenting an appropriate model to simulate tritium uptake and retention in Be, under ITER-relevant conditions. Our intent is to bring together all relevant information in one publication that pertains to assessment of tritium uptake and retention in Be used in tokamak PFC applications.

In Section 2, we first consider the utilization of beryllium in the design of tokamaks, focusing particularly on the ITER. This design is presently considered, by many, to be representative of fusion power-producing machines that will be developed, though admittedly, it is still embryonic for a commercial power plant design. In Section 2.1 the design features of ITER Be components are considered, and in Section 2.2 we review expected operational conditions.

Section 3 provides a detailed compilation and review of the experimental data base for hydrogen uptake and retention in Be. We consider, in Section 3.1, experimental data that were measured for pure Be, including fully-dense, consolidated powder metallurgy (CPM) Be, ingot metallurgy Be foils, and plasma-sprayed Be. Recent results are included from experiments with ion-beam systems, linear plasma simulators, and tokamak plasma environments. Section 3.2 presents the results of experiments to investigate hydrogen uptake in C/Be mixed material layers. The retention of hydrogen during co-deposition of sputtered Be and hydrogen were investigated in experiments that are reviewed in Section 3.3. Microstructural evolution in hydrogen-implanted beryllium is discussed in Section 3.4, and the effects of neutron irradiation on tritium production and retention is discussed in Section 3.5.

In Section 4 we present the results of different strategies for modeling the uptake and retention of hydrogen in Be. Both a conventional diffusion/recombination model and a newly developed saturation model are applied. The results of model calculations for ITER-relevant conditions are presented and compared with the experimental data base.

Finally, Section 5 summarizes the key findings of this work. Observations are presented regarding the experimental data review and the development of an uptake/retention model that is consistent with the experimental data. Factors that influence the uptake and retention of tritium in Be are emphasized and guidance is proposed to enable realistic model prediction of tritium inventories for ITER-relevant conditions. In addition, areas requiring further research are identified.

2. Beryllium utilization as a plasma-facing material

The ITER tokamak is envisioned to be the next major step in the world's fusion program from the present generation of tokamaks, designed to study fusion plasmas with the reactor relevant range of plasma parameters (see key features and parameters in Tables 1 and 2). ITER engineering design has been completed to provide ITER with the capability to achieve sustained ignition, and extended-duration fusion burn in deuterium–tritium (DT) plasmas with reactor-relevant engineering features that include superconducting magnet systems, remotely-maintainable in-vessel nuclear shielding, and PFCs with steady-state power and particle exhaust capabilities. A cross-sectional view of ITER is shown in Fig. 1 [7]. The PFCs in ITER have to cope with severe operating conditions, and high-erosion rates limit their lifetime. Their design has been recognised as among the most challenging problems confronting the ITER design. Present planning is to use beryllium for the plasma-facing material on the FW, including the limiter, and on the upper baffle modules. The lower baffle modules and many surfaces in the divertor, at the bottom of the plasma chamber, will be faced with

Table 1
ITER design parameters

Parameter	Value
Major/minor radius	8.14/2.80 m
Plasma configuration	Single null divertor
Vertical elongation/triangularity (95% flux)	1.6/0.24
Plasma volume	$\sim$2000 m^3
Plasma surface area	$\sim$1200 m^2
Nominal plasma current	21 MA
Toroidal field	5.68 T (at $R = 8.14$ m)
MHD safety factor (q95)	$\sim$3.0 (at 21 MA)
Fusion power (nominal)	1.5 GW
Average neutron wall loading	$\sim$1 MW/m^2 (at 1.5 GW)
Poloidal field system flux swing	$\sim$530 Wb
Flux swing for burn	80 Wb (at 21 MA)
Burn duration (ignited, inductive drive)	1000 s
Toroidal field ripple (peak/average)	0.7%
Auxiliary heating power	100 MW

Table 2
Design parameters and operating conditions of the PFCs in ITER (Basic Performance Phase, Update 1 April 1998)

Component	Surface area* (m^2)	Surface mat'l/ thickness (mm)	Heat flux (MW/m^2)	Operational temp. (front/back) (°C)	Ion/atom flux ($D+T/m^2s$)	Energy (eV)	Fast neutron flux[k] (n/m^2 s)	Lifetime (pulses[l]/dpa)
First wall								
Primary first wall	1025[a]	Be/10 mm	0.25[d]–0.5[e]	285/245[d]	10^{19}–10^{20}	100–500	$1.9–2.3 \times 10^{18}$	10^4/0.8–1 (Be)
Start-up limiter	8.5[b]	Be/4–5 mm	~8[f]	790/360[i] 190/170[j]	10^{21}–10^{22i}	100–500	2.3×10^{18}	$<10^4$/1 (Be)
Upper baffle	80	Be/10 mm	1[d]–2[e]	483/295[e]	10^{19}–10^{20}	100–500	2×10^{18}	10^4/1 (Be)
Lower baffle	109	W/10 mm	1.5[d]–3[e]	640/360[e]	10^{20}–10^{21}	100	1.1×10^{18}	10^4 /0.3–0.5 (W)
Divertor								
Lower target	74	CFC/< 20 mm	< 10[g]–20[h]	1280/340[g]	$<10^{24}$	<5	$4–6 \times 10^{18}$	3×10^3/0.2–0.3 (C)
Sidewall	79	W/15 mm	2[d]–5[e]	460/240[d]	10^{21}–10^{22}	5–100	$0.6–1.1 \times 10^{18}$	3×10^3/0.3–0.5 (W)
Dome	84	W/10 mm	1[d]–5[e]	315/210[d]	10^{21}–10^{22}	5–100	$0.6–1.1 \times 10^{18}$	3×10^3/0.3–0.5 (W)
Cassette liner	90/400[c]	W/(louver)	0.1–0.7	1000–250[m]	$<10^{23n}$	<1	$3.5–4.0 \times 10^{17}$	3×10^3 /0.1–0.2 (W)

* The total area of the plasma facing surface is about 1550 m^2. No asymmetry of the plasma conditions of the inner and outer divertor leg is considered. [a] including port limiter; [b] start-up limiter modules occupy two mid-plane port; [c] surface area of the louvers (see text); [d] design average heat flux (at 1.5 GW); [e] design peak value at any condition; [f] during start-up. During flat-top burn the limiter will experience the same load as the primary first wall; [g] peak load expected during normal semi-detached conditions; [h] peak load expected during off-normal transients (10% frequency, 10 s duration); [i] during limiter operation; [j] during divertor operation; [k] $E > 0.1$ MeV; [l] 1000 s duration; [m] For a given input power density, the temperature varies then from the corner of the chevron to the copper part of the stem.For the case with 0.1 MW/m^2 the maximum temperature for W is 250°C while the stem remains at about 175°C. At 0.7 MW/m^2 the maximum W temperature is 1000°C while the stem is at about 270°C. [n] Molecular hydrogen species dominant at very low energy: $\Gamma_{H_2} \gg \Gamma_H$.

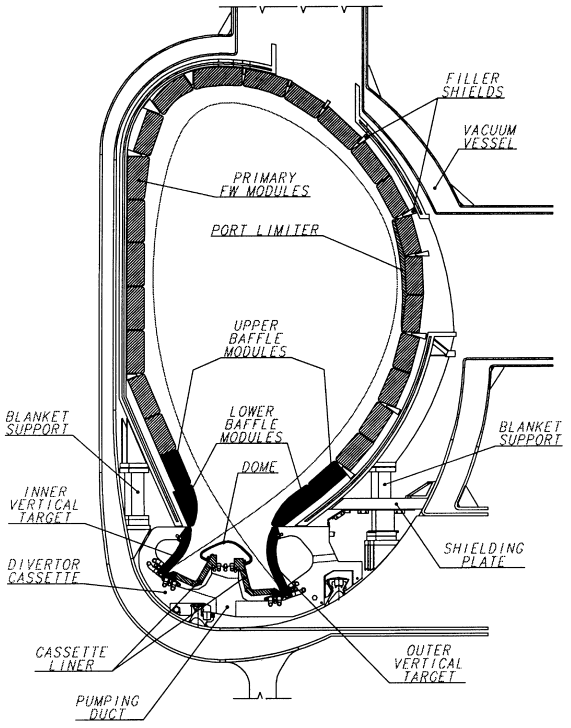

Fig. 1. Cross-section of ITER showing the major components.

tungsten, while the highest heat flux surfaces, which intersect the scrape-off-layer (SOL) at the lower portion of the inner and outer vertical targets, will be made of a carbon fiber composite (CFC) material. The vertical target configuration is being tested on existing tokamaks (Alcator C-Mod, JET, and ASDEX Upgrade).

2.1. In-vessel components: configuration and materials

Inside the vacuum vessel, the FW and the blanket shielding modules are mounted on a double wall permanent back plate attached to the vessel. The segmentation of the shield modules, shown in Fig. 1, is presently dictated by the weight limit of ~4.3 t per module imposed by the remote maintenance equipment, the dimensions of the equatorial port opening, and the desire to minimize the number of modules.

- The *primary modules* have a FW designed to tolerate a heat load of 0.5 MW/m^2, and are in direct contact with the plasma only during off-normal events. Beryllium (S65C) is used here as the plasma facing armor material at the primary FW, because of its plasma compatible low atomic number, and its ability to protect the underlying FW structures from the off-normal thermal loads. It also offers the prospect of repair by plasma spray. The specified Be thickness of 10 mm is a compromise between maintaining reasonable maximum stress during normal operation and accommodating off-normal transient energy deposition (60 MJ/m^2 as maximum for a hot vertical displacement event).
- The portion of the FW adjacent to the divertor cassette (located opposite the X-point) consists of a set of modules referred to as *baffles*. Their function is to spread the flux of recycling neutrals along the length of the divertor plasma and to aid in the transfer of the plasma pressure to the walls by ion–atom inelastic and charge-exchange (CX) collisions. The baffle modules are not normally in contact with the plasma, but are subject to moderate heat loads caused by MARFEs (Multifaceted Asymmetric Radiation from the Edge) and the CX flux arising from neutral-plasma interactions near the entrance to the divertor channel, and are designed to accommodate heat loads up to 3 MW/m^2. Beryllium (S65C) protects the upper regions of the baffle, while W is used in the lower baffle near the divertor because of the elevated particle and heat fluxes which would cause excessive erosion rates on Be. The beryllium thickness in the BPP is planned to be 10 mm.
- The *port limiters* are located in the equatorial ports for improved maintainability. They see a much higher heat flux than the blanket modules, possibly up to ~10 MW/m^2 during start-up and shutdown, and are designed to provide an acceptable critical heat flux (CHF) margin during operation. The limiter coolant is integrated with the divertor cooling system, with the objective of connecting those components with copper internal cooling channels, with their potential corrosion problems in a predominantly stainless steel circuit, as well as connecting the highest and most uncertain heat fluxes, which do not coincide in time during a burn pulse, to a single cooling system. The specified Be thickness is 4–5 mm.

To summarize, in the present design, beryllium has been chosen as the armor material for ~80% of the total surface exposed to the plasma (primary wall, upper baffle and as primary option for the port limiters) on the basis of low main plasma pollution, absence of chemical sputtering, oxygen gettering capability, and possibility of armor repair. S-65C beryllium was selected as the reference grade (DShG-200 is the back up) because of its resistance to thermal fatigue, availability, and previous experience in JET. Its high-sputtering rate makes beryllium less suitable in areas where CX sputtering is the dominant erosion mechanism (lower baffle, upper vertical target); here, W provides the best erosion lifetime. In areas hit by high-thermal fluxes during normal operation and large energy deposition during plasma instabilities (lower vertical target, dump plate), carbon fiber reinforced carbon (CFC) is selected because CFC can resist very high-heat fluxes and does not melt. However, its use has to be restricted to these regions, because of the problems of chemical erosion

and tritium retention, especially in the co-deposited layers.

It was clear from the beginning that the use of C-based materials would exacerbate the problem of tritium co-deposition. Additionally, the simultaneous use of Be, C, and W introduces significant uncertainties into the operation of a tokamak like ITER. Erosion and redeposition phenomena are expected to generate complex carbon-bearing mixed-material layers whose behavior in terms of erosion, tritium retention and removal cannot be predicted from present laboratory experiments. While the development of models for simulating these phenomena has only just begun, current laboratory data indicate that these effects can be significant and that they are strongly influenced by surface chemistry.

Present-day tokamak experience indicates that the FW is an area of net-erosion while the divertor, except during off-normal events, is an area of redeposition, with some poloidal asymmetry in the divertor (the outer leg is an area of net erosion and the inner leg of net redeposition). Although extrapolation of these trends to ITER is still subject to debate, it is expected that mixed-materials in ITER would play a major role in the divertor, e.g., Be on C, and C on W. However, the occurrence of a disruption could transiently determine the outflux of C from the divertor and its deposition onto Be walls.

2.2. Operational conditions

Operation in ITER is articulated in two main operation phases: the BPP and the Enhanced Performance Phase (EPP). Each is planned to last about 10 yr. For the BPP, plasma operation will be preceded by a year of integrated commissioning of the sub-systems followed by a few years of initial operation in hydrogen to gain initial operating experience in a non-radioactive environment. Then there will be a brief deuterium (D) phase before proceeding to operation with a DT mix. Various operational modes are envisaged, including ohmic and additionally heated pulses, 1000 s ignited pulses, and longer pulses assisted by current drive. A detailed operational plan for the EPP has not been developed because it will depend on the plasma performance and operating experience obtained during the BPP.

The set of nominal design parameters and operation conditions adopted for the analysis is given in Table 2. The FW and baffle will not be changed during the BPP, so a lifetime of about 8×10^6 s is assumed based on Table 2. The divertor is assumed to be changed out at the end of $\sim 3 \times 10^6$ s (about 2000–3000 full-power discharges).

3. Review of hydrogen retention data

In this section we review experimental measurements that have been made to understand the processes of hydrogen retention in beryllium. Deuterium and tritium ions and charge-exchange neutral atoms will implant into plasma-facing surfaces. Most of these atoms will return to the plasma but some will diffuse to a greater or lesser extent into the bulk of the beryllium. Traps inhibit release of these isotopes. Return of implanted atoms to the plasma has long been believed to be governed by recombination at the surface [8,9]. Lately, that view is changing for some sets of conditions [10]. Proper understanding of the processes of tritium implantation, retention, and release together with the ability to properly extrapolate/interpolate to conditions relevant to ITER or other fusion machines is important in evaluation of tritium recycling to the plasma and estimation of the tritium source term in accidents.

The main tokamak experience with beryllium as a plasma-facing material was in JET. There it was found that the addition of beryllium to the interior of the vacuum vessel (both as an evaporated film on the carbon tiles lining the vessel and subsequently with solid tiles in the limiter region) resulted in the need for more than twice the deuterium/tritium fueling rate compared with that needed when the surfaces were only carbon. They also saw a 2- to 3-fold increase in the fuel gases released in the first 600 s following the discharges. The hydrocarbon and CO_2 fraction in those gases also sharply declined after beryllium introduction [4]. That behavior appears to be at least in part a consequence of the greater diffusivity of beryllium for transport of implanted atoms beyond the implantation depth and back, though chemical processes are also obviously important.

Studies have sought to understand the processes of implantation-driven diffusion, trapping, and recombination or release at the surface. Some of these were noted by Wilson et al. [1], and subsequent reviews have been presented by Billone et al. [11] and by Khomutov et al. [12]. More recently, a number of new experiments have been performed at higher ion fluxes revealing the important role of high (of order 10^{20} m^{-2}/s or greater) ion flux bombardment on saturation phenomena in beryllium [13]. (Saturation had been observed in oxidized beryllium by Langley [14] in 1979, but saturation effects were not included in simulations until quite recently.) While most investigations have employed relatively pure beryllium, in ITER, it is possible that beryllium surfaces will be contaminated with carbon or other impurities from the divertor and elsewhere in the vacuum vessel. Carbon has been shown to have an effect on retention and release of hydrogen isotopes from beryllium [15]. Further, if oxygen is present, beryllium surfaces may develop oxide layers in which hydrogen isotopes may become co-implanted [16]. In this section we will first consider experiments on pure beryllium, then we will address issues pertinent to mixed materials and co-deposited layers. The data considered here are mainly those with applicability to ITER-like conditions of

Table 3
Compilation of experimental data for retention of implanted hydrogen isotopes in Be

Data set	Facility	Ion exposure	Ion energy (keV)	Ion flux (D/cm^2 s)	Fluence (D/cm^2)	Specimen temperature (°C)	Retention measurement	Specimen description	Refs.
SNL/LANL-TPE	SNL/LANL-TPE	Plasma	0.1	1×10^{17}–3×10^{18}	1×10^{20}–1×10^{22}	100–800	TDS-tritium	Brush Wellman S65	[24]
PISCES-B-1	UCSD-PISCES-B	Plasma	0.1	1.5×10^{17}–1.6×10^{18}	2.7×10^{20}–3.5×10^{22}	200, 500	TDS-deuterium	Brush Wellman	[26]
PISCES-B-2	UCSD-PISCES-B	Plasma	0.1	1.5×10^{17}–9×10^{17}	1.1×10^{21}–6.5×10^{21}	200, 500	NRA-deuterium	Brush Wellman	[26]
PISCES-B-3	UCSD-PISCES-B	Plasma	0.1	8×10^{17}–1×10^{18}	5.8×10^{21}–7.2×10^{21}	40, 540	TDS-deuterium	Plasma-sprayed Be	[26]
DIII-D (DiMES)	DIII-D DiMES	Plasma	0.3	3.0×10^{18}	1.2×10^{19}–4.2×10^{19}	77–177 (Avg. 130)	NRA-deuterium	Evaporated Be film on graphite	[28]
JET-NB	JET	Neutral beam	60	4.5×10^{16}	2.0×10^{19}	120	NRA-hydrogen	Brush Wellman S65	[29]
INEEL	INEEL	Ion beam	1	4.0×10^{15}	1.6×10^{19}–1.8×10^{19}	200–400	TDS deuterium	BW Electrofusion IF-1 foil	[22]
UTIAS	UTIAS U. Toronto	Ion beam	1	1.0×10^{16}	2×10^{17}–4×10^{20}	27	TDS deuterium	Brush Wellman PF-60 foil	[17]
SNLARF	SNLA	Ion beam	1.5	1.0×10^{14}	3×10^{14}–8×10^{17}	470, 600	NRA-deuterium	Russian TIP-30	[19]
SNLAUS	SNLA	Ion beam	1.5	1.0×10^{14}	1.2×10^{14}–5.1×10^{17}	500, 600	NRA-deuterium	Kawecki-Berylco Electropolished	[19]
SNLAW	SNLA	Ion beam	1.5	1.0×10^{14}	5.0×10^{17}	25, 200	NRA-deuterium	Kawecki-Berylc Electropolishedo	[18]
Alimov	Inst. Phys. Chemistry Moscow	Ion beam	9	$\sim 10^{16}$	6×10^{15}–9×10^{18}	25, 430	Sputter desorption RGA&SIMS	Russian TIP-30	[21,20]
Moller	Max Planck Garching	Ion beam	0.06–20	5×10^{13} at 1 keV to 1.5×10^{15} at 10 keV	$\sim 2 \times 10^{18}$	25, 250, 450	NRA	Brush Wellman S65 Polished, etched	[23]

high-particle flux to surfaces at low to moderate temperatures. We will also consider microstructural evolution and neutron effects.

3.1. Retention in pure Be

Retention data for hydrogen isotopes in beryllium are usually obtained from experiments in which atoms are implanted or otherwise introduced to the material followed by thermal desorption or nuclear reaction methods for deuterium; for tritium, sample dissolution and scintillation counting methods are sometimes used. Data were obtained from experiments with ion beams [17–23], linear plasma devices [24–27], a tokamak divertor plasma [28] and tokamak neutral beams [29]. Results from the linear plasma devices are of particular relevance to ITER because these devices best simulate the plasma conditions expected for ITER PFC materials. Those data are emphasized here. Most beam experiments have ion energies well above the displacement threshold energy for beryllium and may produce effects not present in the lower energy environments of the linear plasma devices or in ITER. The results from the lower fluence ion-beam experiments are included because they have historically served as important reference data from which hydrogen transport and retention parameters were derived and from which transport/retention models were developed. Table 3 provides a summary of various experiments and details the implantation conditions, the method of measuring retention of implanted deuterium or tritium, and the type of specimen tested. The data were taken from published reports or papers and from other more recent data that are being prepared for publication. Table 4 summarizes material specifications for the CPM and other forms of beryllium that were tested in the various experiments.

Typically, two methods for measuring retained deuterium or tritium were used; thermal desorption spectroscopy (TDS) and nuclear reaction analysis (NRA). The two approaches differ significantly. In a TDS measurement, gases released from the implanted sample are measured as the sample is heated to temperatures between 800°C and 1200°C. In an NRA measurement, the sample is interrogated with a high-energy particle beam, and nuclear reaction products resulting from interactions with deuterium or hydrogen are measured to establish the hydrogen isotope concentration in the sample. NRA is usually limited to probing the sample to a depth of a few micrometers.

Figs. 2–7 display the reported hydrogen retention data for pure Be in a variety of ways; as functions of ion energy, specimen temperature, and particle fluence. Data-set labels in the figures correspond to the identifiers in column 1 of Table 3. In Figs. 2–5, the results of all experiments for pure Be considered here are included in the data comparisons. Based on these comparisons, a selected set of high-fluence results are presented in Figs. 6 and 7, because they best represent the retention conditions that are most relevant to ITER. Figs. 6 and 7 also include the results of recent experiments for plasma-sprayed Be [26].

Fig. 2 presents the retention results as a function of the implanting deuteron energy, where the deuteron energies range from 0.06 to 60 keV/D. The temperature range in degrees Celsius covered by the experiments is identified by the numerical values in the legend identifiers. The three curves in the figure are power function fits to the Moller data [23] corresponding to

Table 4
Specifications for Be material that was used in experiments

Type	Be (min %)	BeO (max %)	Impurities (appm)	Grain size (μm)	Fabrication method	Surface finish
Brush-Wellman S65	99	1	Al(600), C(1000), Fe(800), Mg(600), Si(600), others(400)	10	Impact-ground powder, vacuum hot pressed	3 μm RMS
BW Electrofusion IF-1 foil	99.8	300 appm	Al(100), Fe(300), C(300), Mg(60), Si(100), Cr(25), Cu(50), Mn(30), Ni(200), Ca(200), Zn(100)	–	Extruded, hot-rolled Be ingots cast from vacuum-melted electrolytically refined Be flake	Best-buffed, ~0.3 μm RMA
Brush Wellman PF-60 foil	99.5	0.6	Fe(100), C(300), Al(70), Mg(15), Si(100), Mn(3), Cu(3)	–	Hot-rolled, hot-pressed powder metallurgy product	1.6 μm RMS
Russian TIP-30	97.7	2.2	–	20	Hot isostatic pressed	–
Kawecki–Berylco	99.3	1.0	C(200), Fe(190), Al(60), Mg(60), Si(80), Cr(10), Co(5), Cu(50), Pb(1), Mn(20), Mo(10), Ni(180)	15	Cold isostatic pressed followed by hot isostatic pressed	Electropolished

measurements at 25°C, 250°C and 450°C. Typically, the plotted data correspond to the maximum fluence exposures for an experiment. Retention trends with ion energy are obvious; retention increases with ion energy. However, there are apparent discrepancies between the different data sets at comparable ion energies. These are most likely related to the different fluxes and fluences to which the specimens were exposed in the various experiments. For the highest flux and fluence experiments (SNL/LANL-TPE [24], PISCES-B [26,27], UTIAS [17] and INEEL [21]), the retained quantities of deuterium are higher than those for the other experiments at comparable temperatures but with lower fluxes and fluences.

A comparison of the retained deuterium as a function of specimen exposure temperature is given in Figs. 3 and 4. Ion energies for each experiment are identified by the numerical values in the legend labels. Fig. 3 compares the results from experiments for deuteron energies of 0.1 and 0.3 keV. The Moller data [23] correspond to maximum values measured in ion-beam experiments with 0.1 keV/D. Results from the linear plasma devices are those identified as SNL/LANL-TPE [24] and PISCES-B [26,27], both conducted with 0.1 keV plasma ions. Two data points correspond to experiments with the DiMES probe in the DIII-D divertor plasma in which impinging ions had 0.3 keV energy [28]. Fig. 4 presents the results from ion-beam experiments [17–23] in which the deuteron energy ranged from 1 to 10 keV. Both figures illustrate the reduction in retained quantity as the specimen temperature is increased. Discrepancies between the retained quantities from the various experiments probably correspond to differences in ion energy, ion flux and ion fluence and to differences in the materials tested.

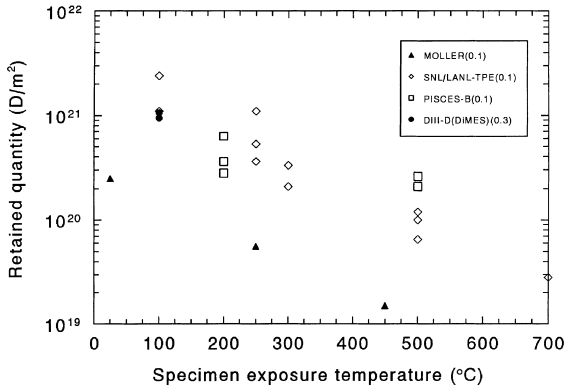

Fig. 3. Comparison of deuterium retention data as a function of specimen temperature in experiments for which the implanting ions had energies of 0.1 or 0.3 keV. Ion energies are indicated by the numerical values attached to the experiment identifiers in the legend box. Particle fluences for the Moller experiment were substantially less than those for the other experiments.

An attempt to remove the bias associated with different ion energies is provided by the adjusted data plotted in Figs. 5–7. In these figures, the reported retention data were adjusted to account for range differences in experiments that use different energy ions. Adjustment factors used to place the retention data on an equivalent ion-energy scale were computed from ion-range calculations with the TRVMC code [30]. Range

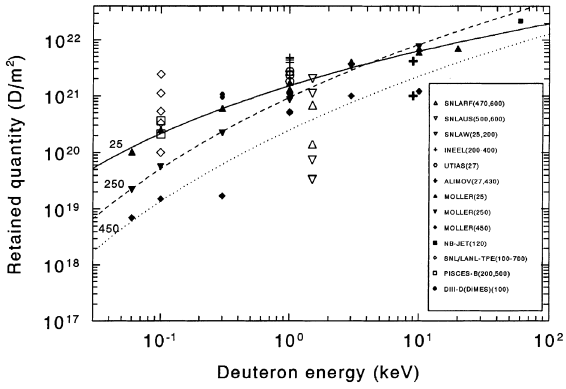

Fig. 2. Comparison of selected deuterium retention data from various experiments (SNARF and SNLAUS [19], SNLAW [18], INEEL [22], UTIAS [17], Alimov [20,21], Moller [23], NB-JET [29], SNL/LANL-TPE [24], PISCES-B [26,27] and DIII-D(DiMES) [28]). The data are plotted as a function of deuteron energy, similar to that found in Moller [5]. The solid and dashed curves are fits to the data of Moller, for specimen temperatures of 25°C, 250°C and 450°C. A numerical value in parenthesis next to the legend identifier indicates the specimen temperatures or temperature range during implantation for the experiments. Particle fluences during implantation vary considerably from experiment to experiment.

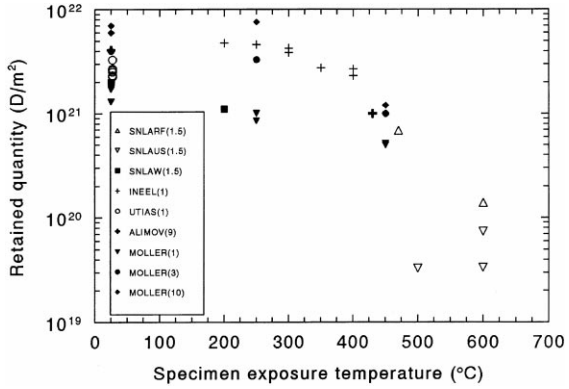

Fig. 4. Comparison of deuterium retention data as a function of specimen temperature for experiments in which the ion energy ranged from 1 to 10 keV. The ion energy in an experiment is indicated by the numerical value attached to the experiment identifier in the legend box. Particle fluences varied substantially from experiment to experiment.

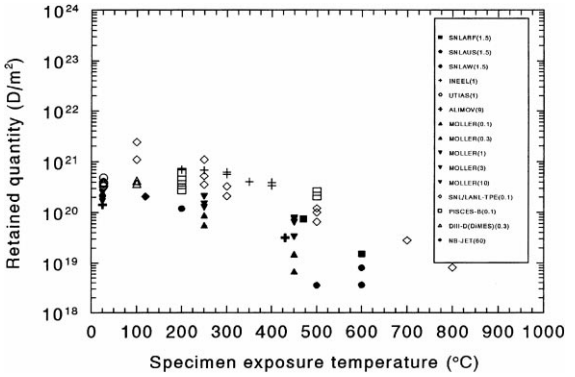

Fig. 5. Comparison of *adjusted* deuterium retention data as a function of specimen temperature for experiments (SNARF and SNLAUS [19], SNLAW [18], INEEL [22], UTIAS [17], Alimov [20,21], Moller [23], NB-JET [29], SNL/LANL-TPE [24], PISCES-B [26,27] and DIII-D(DiMES) [28]) in which the incident ion energy ranged from 0.1 keV to 60 keV. The ion energy in an experiment is indicated by the numerical value attached to the experiment identifier in the legend box. Retention data were *adjusted to correspond to an equivalent ion energy of 100 eV* for experiments in which the ion energy was greater than 100 eV. Adjustment factors were obtained from TRVMC calculations of the ranges of the incident particles as a function of energy. Values for SNL/LANL-TPE, PISCES-B, DIII-D (DiMES), UTIAS and INEEL, the open symbols and light crosses, are from retention experiments having much higher fluences (10^{23} to 10^{27} D/m^2) than the other cited experiments represented by solid symbols and bold crosses for which the fluences were much lower (10^{19} to 2×10^{22} D/m^2).

results are presented in Table 5 for deuteron energies that are relevant to the data comparison. The range results are tabulated as mean values, and values corresponding to stopping of 99%, 99.9%, 99.99% and 100% of 100 000 incident particles. Table 6 details the ratios of the range data for ion energies relative to 0.1 keV and relative to 1 keV. In the adjustment of the deuterium retention data, the range ratios corresponding to 99.9% were used. For example, a retention value that was measured for 1 keV ions was divided by 6.8 to place the retention on an equivalent 0.1 keV scale. This approach for adjusting the retention is based on the following assumptions: (1) implanted ions saturate the implantation zone with an atomic concentration that is temperature sensitive but otherwise is the same for all ion energies of interest here, (2) the implantation zone thickness varies with ion energy and corresponds to the depth over which 99.9% of the implanting particles are stopped, and (3) there is no significant thermal transport of implanted ions deeper than the implantation zone during the time of the experiments. For room temperature experiments, these assumptions seem reasonable. For experiments with samples at elevated temperatures, the approach is less accurate. Inventories resident in the implantation layer would be reduced at higher temperatures, but there would be an increased inventory due to diffusion into the bulk. No attempt was made at such sophistication in the correlation of the data.

Fig. 5 presents the retention data as a function of specimen exposure temperature for data adjusted to be equivalent to 100 eV. The original ion energy for a particular data set is identified by the numerical value in parenthesis attached to the experiment identifier in the figure legend. Differences in fluence conditions are indicated by the symbols used to plot the retention data. Data corresponding to fluences between 10^{19} and 2×10^{22} D/m^2 are identified by the solid symbols and by the bold crosses. Data corresponding to fluences from 10^{23} to 10^{27} D/m^2 are identified by the light crosses and the open symbols. We observe that Fig. 5 illustrates a fluence-related difference in the retention results, with the retention values corresponding to lower fluence experiments being much lower than those from the higher fluence experiments. In particular, it shows that for the higher-energy ion- and neutral-beam experiments (Alimov (9 keV), Moller (10 keV), and JET-NB (60 keV)), the fluence required to obtain a saturation concentration throughout the implantation zone is considerably higher than that achieved in the experiments.

A final comparison of the retention data is given in Figs. 6 and 7. In these figures, a reduced set of retention data is plotted, namely, data corresponding to the highest fluence ion-beam experiments, data obtained from the high-flux linear plasma devices and data obtained from auxiliary tokamak facilities. The results are plotted with all data adjusted to be equivalent to 100-eV

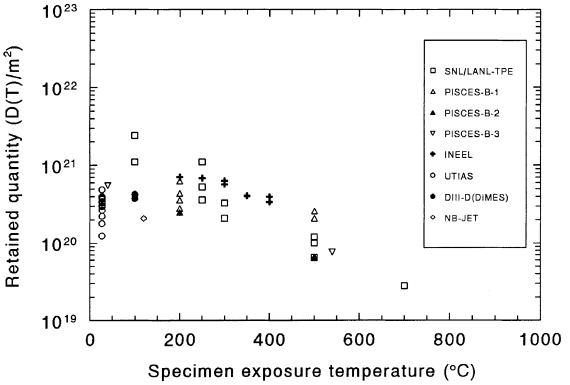

Fig. 6. *Adjusted* deuterium retention data for Be as a function of specimen exposure temperature for a selected set of high fluence experiments. Data were obtained from experiments in which Be specimens were exposed to deuterium ions from laboratory ion beams (INEEL [22], UTIAS [17]), linear plasma devices (SNL/LANL-TPE [24], PISCES-B [26,27]), tokamak divertor plasma (DIII-D(DiMES) [28]), and tokamak neutral beam (NB-JET [29]). The data have been *adjusted to correspond to equivalent 100 eV deuterium ions.*

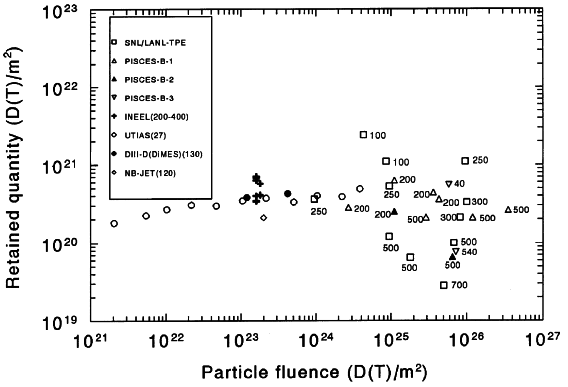

Fig. 7. *Adjusted* deuterium (tritium) retention data for Be as a function of incident particle fluence for a selected set of high fluence experiments. Retention data were obtained from experiments in which pure Be specimens were exposed to deuterium ions from laboratory ion beams (INEEL [22], UTIAS [17]), linear plasma devices (SNL/LANL-TPE [24], PISCES-B [26,27]), a tokamak divertor plasma (DIII-D(DiMES) [28]), and a neutral beam (NB-JET [29]). The data have been *adjusted to correspond to an equivalent 100 eV deuterium ion*. Numerical values next to the open squares, open triangles and closed triangles correspond to specimen exposure temperatures, in degrees Celsius, for Be tested in the SNL/LANL-TPE and PISCES experiments. Three data sets are presented for PISCES-B: PISCES-B-1 corresponds to thermal-desorption of plasma-exposed S65 Be, PISCES-B-2 corresponds to retention based on nuclear reaction analysis for plasma-exposed S65 Be, and PISCES-B-3 corresponds to thermal-desorption analyses for plasma exposure of plasma-sprayed Be. Specimens tested at 500°C in PISCES-B developed a thin carbon surface layer during plasma exposure. Specimens tested in the DIII-D divertor plasma developed 2–4 nm thick carbon surface layers. Typical particle energies and fluxes for these experiments are found in Table 3.

ions. In addition to results for fully-dense, pure Be, these figures include the results from recent PISCES-B experiments for plasma-sprayed Be (PISCES-B-3 in the figures). They also include PISCES experiment results in which NRA was used to profile the concentration of implanted deuterium and to measure the deuterium areal densities (PISCES-B-2) for pure Be specimens exposed to the PISCES-B plasma at 200°C and 500°C. The data are plotted as a function of specimen exposure temperature in Fig. 6 and as a function of incident particle fluence in Fig. 7. In Fig. 7, temperatures corresponding to the SNL/LANL-TPE and PISCES-B data are given near the data points. Sample temperature ranges for the other experimental data are indicated by the numerical values in parenthesis next to the legend identifiers.

These plots may appear complicated from a visual perspective. However, the data comparisons indicate the following:

1. In a global sense, the ion-beam data and the plasma data are reasonably consistent over a temperature range of 27°C–500°C, provided the results are compared on a basis that accounts for differences in ion ranges.
2. D(T) retention does not appear to be a strong function of fluence, provided that the fluence is above 10^{22} D(T)/m^2 for ion energies of 1 keV or less.
3. D(T) retention varies more strongly with temperature and is reduced by about one order of magnitude as the temperature varies from 27°C to 700°C.
4. Measured D(T) retention for ITER-relevant plasma exposure conditions begins to saturate at about 1×10^{21} D(T)/m^2 in Be. In contrast, if one assumes that tritium uptake and retention are governed by bulk diffusion and surface recombination, as per previous predictions of tritium inventory in the ITER FW or baffle Be, the retention is orders of magnitude larger.
5. The amount of retained D measured by nuclear-reaction-analysis is comparable to the amount based on thermal desorption for samples exposed at 200°C in PISCES, but the NRA results are three times lower than TDS data for 500°C plasma exposure, indicating possible D transport into the bulk, beyond the range probed by NRA.
6. For comparable test conditions, PISCES-B plasma-exposure results in less D(T) retention in plasma-sprayed Be than that in fully dense Be.

Table 5
TRVMC calculation of ion ranges for D implantation into Be

Energy (eV)	Mean range (nm)	99% range (nm)	99.90% range (nm)	99.99% range (nm)	100% range (nm)
100	2.8	6.8	8.2	9.1	9.6
200	5.3	12.4	14.5	16.2	17.2
300	7.8	17.5	20.5	22.7	26.1
500	12.9	27.4	31.3	34.5	36.9
1000	25.6	49.4	55.5	59.4	63.5
1500	38.4	69.5	76.0	80.5	85.0
3000	74.9	119.5	129.5	136.5	142.5
9000	197.1	265	278	288	292
10,000	214.8	284	295	305	310
60,000	762.8	850	865	875	885

Table 6
Ratios of D ion range values in Be relative to 100 eV and to 1000 eV values

Ion energy ratio	Mean	99%	99.9%	99.99%	100%
300/100	2.77	2.57	2.5	2.5	2.72
500/100	4.59	4.03	3.82	3.79	3.84
1000/100	9.14	7.26	6.77	6.53	6.62
1500/100	13.7	10.2	9.27	8.85	8.85
3000/100	26.8	17.6	15.8	15.0	14.8
9000/100	70.4	39.0	33.9	31.6	30.4
10,000/100	76.7	41.8	36.0	33.5	32.3
60,000/100	272.4	125	105	96.2	92.2
1500/1000	1.50	1.41	1.37	1.36	1.34
3000/1000	2.93	2.43	2.33	2.30	2.24
9000/1000	7.70	5.36	5.01	4.85	4.60
10,000/1000	8.39	5.75	5.32	5.14	4.88
60,000/1000	29.8	17.2	15.6	14.7	13.9

We now turn to concentration profiles of implanted atoms in the beryllium. Several recent experiments have explored concentration profiles of deuterium implanted into beryllium, including the effects of microstructural changes on those profiles. These will now be considered.

For some of the Be samples exposed to the PISCES-B plasma at temperatures of 200°C and 500°C, deuterium retention was measured using NRA, and the composition of the surface was analyzed by Rutherford-backscattering (RBS) analysis. These experiments are identified in Table 3, and the deuterium areal densities are plotted in Figs. 6 and 7 with the label PISCES-B-2. The NRA measurements were made using the ^{3}He(d,p)α reaction with the ^{3}He analysis beam incident normal to the sample surface. The yield of energetic protons was counted as a function of the analysis beam energy between 0.3 and 2.4 MeV. The higher beam energies detect D at greater depths whereas protons from the lower beam energies come from reactions with D nearer to the surface. Fig. 8 shows the D concentration versus depth obtained by deconvolution from the measured proton yield versus ^{3}He energy. This figure shows the average D concentration versus depth beneath the surface along the direction of the analysis beam, i.e. normal to the sample surface. The depth scale is obtained from the energy loss of the ^{3}He ions and is therefore in units of mass per unit area. The depth scale is converted to units of distance by dividing by the volume density of the material. The upper scale shows the depth in μm assuming the bulk density of beryllium metal. The total areal density of D, obtained by integrating the concentration over the depth probed by the NRA, is given in the legend box and is plotted in Figs. 6 and 7. For the sample exposed at 200°C the areal density of D measured by NRA is comparable to the D released during thermal desorption. However, the areal density of D measured by NRA on samples exposed at 500°C was about three times less than the amount released from similar samples during thermal desorption. This suggests that at 500°C, D may permeate into the Be beyond the range of the NRA measurement (6 μm) at concentrations below the NRA detection limit (10 appm). At this concentration the D must permeate more than 100 μm to account for the different amounts of D measured by TDS and NRA.

RBS analyses showed that the sample exposed at 500°C had oxide extending to depths of about 1 μm. The

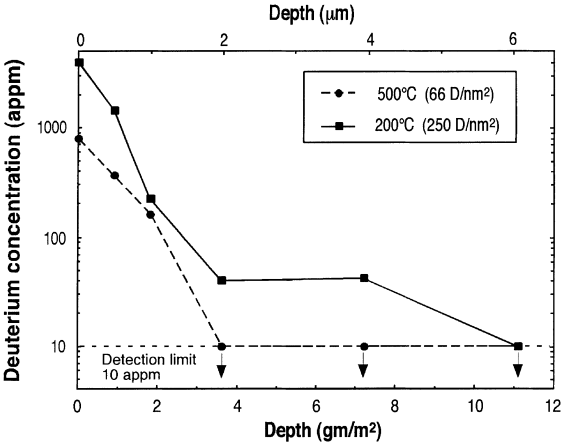

Fig. 8. Deuterium depth profile for Be exposed at 200°C and 500°C to 100 eV ions from the PISCES-B plasma. Deuterium concentrations were measured with NRA. RBS measurements identified an oxide surface layer approximately 14 nm thick for the sample exposed at 200°C and up to 1 μm thick on the sample exposed at 500°C. Optical microscopy revealed that the surface roughness could be as much as 3 μm. Symbols with arrows indicate that the deuterium concentrations for the identified data points are at or below the detection limit of 10 appm. The areal densities computed by integration of the depth-profile curves are given by the numerical values in parentheses in the legend box.

sample exposed at 200°C had a much thinner oxide, only 14 nm thick. These results may indicate that for the 200°C sample the oxide growth rate was sufficiently low that sputtering maintained a clean Be surface during the plasma exposure. However, for the 500°C sample, the rate of oxide growth was apparently greater than the sputter removal rate. One implication of the RBS results is that deuterium implantation may have been into two different materials, Be metal at 200°C and BeO at 500°C. This could affect permeation into the bulk.

The NRA depth profiles show that deuterium in Be exposed to the plasma in PISCES-B extends far beyond the depth to which the D is implanted, which for 100 eV D is less than 10 nm. Examination of the specimens using optical microscopy showed that exposure to the plasma had greatly increased the roughness of the surface. The amplitude of the surface roughness was estimated to be up to about 3 μm on both 200°C and 500°C samples, which is comparable to the depth of D in the NRA profiles. It is highly possible that the observed D depth profile is influenced by the surface roughness and is not simply due to diffusion of D through bulk Be. For example if the roughness is due to the formation of a porous surface layer by precipitation of deuterium into gas bubbles which eventually interconnect, this could lead to a structure in which the D is adsorbed onto the surfaces of the porosity. In any case, the NRA gives the average D concentration versus depth, regardless of the surface microstructure or the mechanism by which the D distribution was produced. Furthermore, the NRA quantitatively measures all the D regardless of its physical state, including D in solid solution, D trapped at defects, D adsorbed on surfaces or molecular D_2 in internal gas bubbles. A further important point is that the integrated areal density of D measured by NRA is not significantly influenced by surface microstructure or composition.

Recent studies by Chernikov et al. [20] included transmission electron microscopy (TEM) on samples of Russian TIP-30 beryllium that had been irradiated with 3 and 10 keV ions to fluences of 3×10^{20}–8×10^{21} D/m^2 at temperatures from ambient to 427°C. By means of secondary ion mass spectroscopy (SIMS) and residual gas analysis (RGA), they were able to evaluate separately concentration profiles for both atomic and molecular deuterium. They found that at 27°C irradiation temperature with 3 keV deuterium ions to a fluence of 3×10^{21} D/m^2, closely spaced few-nanometer-sized deuterium bubbles appeared. Irradiating to a similar fluence with 10 keV deuterons at 427°C, they found that bubbles were several times larger, and labyrinths with channel widths of 100 nm were pervasive in the vicinity of the implantation depth. They further observed that for a 27°C specimen irradiated with 9 keV deuterons to fluences of only 10^{16}–10^{19} D/m^2, both atomic and molecular deuterium were found in nominally equal concentrations of up to 4×10^{21} m^{-3}, growing from the implantation depth, estimated to be 160 nm, and broadening with increasing fluence. The atomic deuterium concentration profile appeared to broaden bilaterally with a high concentration growing at the surface, possibly as a hydroxide, but the molecular deuterium concentration profile strongly favored the implantation side of the implantation zone, falling to zero at the surface. The appearance was that the molecules tended to reside in the region damaged by the implanting ions and probably corresponded to the small bubbles observed by TEM. Similar results have been reported by Yoshida et al. [31]. Hydrogen isotopes exist in both molecular and atomic form in neutron-irradiated beryllium as well [32].

It has been known for several years that beryllium saturates with hydrogen under ion bombardment [18,33]. Guseva et al. [34] exposed Russian TShP beryllium (98.7 wt% Be, 0.9 wt% O, 0.2 wt% Fe) to 5 keV H ions with flux density 6.2×10^{21} H/m^{2}s in the SAPPHIRE facility. They reported that ERD and SIMS measurements of the hydrogen profile showed an unexpected reduction in the inventory of implanted hydrogen and a shift of the spatial distribution of that hydrogen toward the surface with increasing ion fluence. After a fluence of 2.3×10^{23} H/m^2, surface pits were observed to develop mostly along grain boundaries. By 1.2×10^{24} H/m^2 erosion cones were beginning to form, and by 1.5×10^{25} H/m^2 cones had grown to an advanced stage with the surface under the cones taking on a rather amorphous appearance.

Additional insight was gained from the experiments on the TPE. 5 cm diameter disks of hot-pressed and sintered S-65 beryllium, 2 mm thick, were exposed to fluxes of deuterium ions with a 3% tritium tracer. Plasma currents of 0.8 to 9.2 A gave fluxes from 2.5×10^{21} to 2.8×10^{22} (D + T)/m^{2}s at ion energies of about 100 eV. Exposures lasted 1 h with samples maintained at constant temperatures from 100°C to 700°C. Sample temperature was controlled by varying thermal conductance from the back side of the samples and adjusting current to give the preselected temperature. Post-experiment observation of samples under a scanning electron microscope revealed the surface was 'hairy' from formation of many slender and closely spaced sputter-erosion cones.

INEEL experiments [35] conducted in the early 1990s were characterized by implantation fluxes of 5–6 $\times 10^{19}$ D/m^2 s at 1 keV/D and sample temperature of the order of 450 to 500°C. The samples were 25–71 μm thick. The upstream surfaces of the foils were found to have severe damage and pitting to a depth of 1 μm following the experiments, which reached fluences to 1.7×10^{24} D/m^2.

Although the above data comparison provides a reasonable global picture regarding tritium uptake and retention in ITER PFCs that incorporate Be, there are

some differences and discrepancies between the various experimental data sets. A more rigorous assessment of the data should include consideration of the following factors that affect the uptake and retention:

1. the influence of differences in material fabrication, microstructure, and impurity concentrations, especially BeO, on retention;
2. the influence of different ion energies, hence consequent differences in beam-induced damage and trap sites, on retention and the depth of the zone over which the saturation concentration is achieved;
3. the flux and fluence dependence of the saturation concentration, especially for elevated temperature implantations;
4. thermal effects, especially important for elevated temperature implantations, and how they affect transport of deuterium and beam-induced vacancies deeper than the implantation zone and how they affect evolution of the beam-modified microstructure and deuterium retention;
5. the character of the sites at which deuterium is trapped, e.g., BeO sites, vacancy/vacancy cluster defect sites, microscopic voids in which deuterium is trapped as gas bubbles;
6. the role of the surface, especially the extent of BeO coverage, on deuterium uptake and retention;
7. differences in measured deuterium retention that relate to different measurement techniques, e.g., NRA versus thermal desorption.

3.2. Retention in C/Be mixed material layers

Because the present design for ITER includes the use of carbon, tungsten and beryllium in various PFCs, erosion–redeposition phenomena are expected to generate complex mixed-material layers on the PFCs. Consequently, studies have been initiated to investigate hydrogen isotope retention in such layers. This paper includes results that have been reported by Roth et al. [36], Anderl et al. [37], Ashida and Watanabe [15,38,39], Won et al. [40] and Wampler et al. [28] concerning this issue.

Roth et al. [36] studied deuterium retention and release from an amorphous-C:D (a-C:D) layer on a Be substrate. In that work, a 200 nm thick a-C:D layer was deposited on a Be substrate by an RF plasma. Ion-beam analysis confirmed that the D/C ratio was about 0.4 for the layer. The composition of the layer was monitored by RBS and elastic recoil detection analysis (ERDA) during subsequent heat treatment of the coated Be substrate in ultra-high vacuum. These measurements indicated that heating of the sample to 490°C caused Be diffusion into the a-C:D layer, resulting in release of deuterium and formation of Be_2C. The implication of this experiment is that, for a temperature of 490°C, deuterium retention in the a-C:D layer is reduced significantly by formation of Be_2C.

Anderl et al. [37] have approached the study of deuterium uptake and retention in mixed materials by investigating deuterium implantation and release from coated PFC materials. Initial efforts concentrated on carbon-coated Be specimens that were heat-treated in a vacuum to form binary mixtures. These studies entailed preparation, heat treatment and Auger electron spectroscopy (AES) characterization of Be samples coated with carbon with thicknesses of 10, 50, 100 and 130 nm. AES depth-profile measurements for annealed coated specimens indicated that for a temperature of 300°C, no Be diffusion was observed for a 2 h annealing. For a temperature of 400°C, Be diffused in a carbon overlayer at a rate of about 20 nm/h, whereas, for a temperature of 500°C, Be diffusion in the carbon overlayer was quite rapid. At a temperature of 500°C, Be diffusion in a 130 nm thick carbon overlayer was complete in less than 2 h. Based on spot AES analyses, the composition of the mixed layer was approximately 56% Be and 44% C. A more accurate determination of elemental composition would require AES scans over the entire sample area. Nevertheless, the results indicate a possible mixed layer composition of Be_2C and graphitic phases.

Subsequently, both pure Be and annealed, carbon-coated Be specimens were heated to 400°C and exposed to a fluence of about 2×10^{23} D/m^2 of 1 keV D ions at a flux rate of 6×10^{19} D/m^2 s. TDS measurements indicated that, for comparable implantation conditions, the quantity of deuterium retained in the carbon-coated Be sample was about 40% more than that retained in the uncoated samples, and the release of deuterium occurred predominantly at lower temperatures for bare Be than for carbon-coated Be samples. This suggests that most of the deuterium retention was incorporated in the carbon coating.

A comprehensive investigation into the formation and characterization of mixed Be/C and Be/H/C layers as a function of heating in vacuo has been made by Ashida et al. [15,38,39] Three types of samples were tested in these experiments: (1) a 10 nm thick carbon film on a high-purity Be substrate (99.8% Be) produced by deposition of carbon that was evaporated from an arc discharge between two carbon electrodes, (2) high-purity Be plates covered with a carbon film containing hydrogen that was deposited during exposure to an ethylene plasma (13.56 MHz, 40-W, RF discharge with C_2H_4 gas at 40 Pa), and (3) high-purity Be plates implanted with C_2H_4 ions at 5 kV acceleration voltage to a total dose of 2×10^{22} ions/m^2. Changes in the physicochemical properties of the layers were measured as a function of temperature using a variety of techniques: (1) X-ray diffraction (XRD) for structure identification, (2) X-ray photo electron spectroscopy (XPS), Raman spectroscopy (RS) and secondary ion mass spectrometry (SIMS)

for chemical state identification, and (3) TDS to determine gas evolution and retention information.

Experiments for the 10 nm thick evaporated carbon film on pure Be revealed the following properties for this sample type. XRD and RS analyses indicated that the as-prepared carbon layer was amorphous carbon. XPS analysis (measurements of the Be-1s, C-1s and O-1s spectra) indicated that the as-prepared carbon layer was free of Be but most likely contained impurities such as hydrogen, oxygen and/or hydroxide that were chemically bound to carbon. These impurity identifications were confirmed by the SIMS analyses. The source of the impurities was attributed to residual gas pickup from the poor-quality vacuum (1.3×10^{-4} Pa or higher) environment during deposition of evaporated carbon.

Isothermal heating of the sample with a 10 nm carbon film at temperatures between room temperature and 800°C revealed significant changes in the physicochemical properties of the carbon layer. XPS measurements indicated that for temperatures of 600°C and higher, Be diffused into the carbon film and reacted with carbon to form Be_2C and with O to form BeO, with Be_2C being the dominant component in the film. The onset of this film transformation was about 500°C. The XPS measurements indicated that hydrogen and oxygen chemically bound to carbon in the layer were released for temperatures between room temperature and 600°C. This was confirmed by TDS measurements that contained desorption peaks for H_2O near 300°C, for CH_4 and CO at 400°C and pronounced peaks for H_2 at 400°C and 600°C. XRD analyses also identified the formation of Be_2C crystallites at 600°C and above. Negative SIMS analyses, using an Ar–deuterium ion beam, showed that hydrogen isotope atoms were trapped by carbon atoms in the layer but not by the Be_2C.

The results of experiments on the hydrogen-rich carbon layers formed by ethylene discharge or ion implantation were similar to the above results but with some additional physicochemical features for the deposit produced by energetic ion implantation. XRD analysis of the as-prepared deposit from the ethylene discharge indicated no diffraction peaks associated with Be_2C. However, for such samples heated above 600°C, XRD analyses identified the formation of Be_2C crystallites, with the transformation occurring rapidly above 700°C. The XRD analyses indicated that the rate of Be_2C formation was controlled by random nucleation and subsequent growth of Be_2C crystallites at the boundary. TDS measurements for the samples revealed pronounced desorption peaks for H_2 at 400°C and between 500°C and 600°C, with smaller peaks for H_2O at 300°C and for CH_4 and CO at 400°C. In contrast, XPS analysis of the Be sample that was implanted with energetic ions of C_2H_4 identified both BeO and Be_2C phases, as well as amorphous carbon in the as-prepared sample. The formation of the Be_2C phase may be attributed to local mixing and reaction of implanted carbon with surface Be atoms caused by energy deposition and/or transfer during ion bombardment. Heating of the implanted sample to 600°C increased the Be_2C component of the surface layer.

In recent studies with PISCES-B, Won et al. [40] have investigated the formation of mixed-material impurity layers on hot Be exposed to a deuterium plasma. Typically, the mixed-material layer consisted largely of Be (65–55%) intermixed with smaller quantities (35–45%) of C, O and N. Surface analyses indicated a low concentration of Be_2C in the as-formed layers. For a sample exposed to a plasma at 620°C, 26% of the carbon was associated with Be_2C bonds and 74% as C–C bonds. Conditions for formation of the impurity layers and the impact on deuterium retention have been investigated. Formation of the mixed-material impurity layers was found to be dependent on the impurity content of the plasma, e.g. the presence of C and O. This was investigated for carbon. For carbon impurity concentrations of 2% and lower in the plasma, no impurity layers were formed for specimen temperatures at or below 250°C. Carbon impurity concentrations of 10% resulted in impurity layer formation on Be targets even during room temperature exposure. During high temperature, plasma exposures of samples (at and above 500°C), impurity layers formed with plasma impurity concentrations as low as 1%.

Also in this work on PISCES-B [41], deuterium retention measurements were made using TDS for Be samples implanted at a temperature of 500°C during exposure to PISCES-B plasmas with carbon-impurity concentrations of 1–2%. For these impurity concentrations, carbon impurity layers were formed, and the deuterium thermal release behavior included a low-temperature (200–300°C) desorption peak that was not observed from Be samples without an impurity layer. For this experiment with a 1–2% carbon plasma impurity, a 200 nm thick impurity layer was formed after a 20 min exposure, and the deuterium desorbed in the low temperature peak was 16% of the total deuterium retained in the sample.

In addition to these studies that specifically investigated the formation, characterization and hydrogen retention properties of mixed-material layers, earlier work by Wampler et al. [28] observed the formation of carbon over-layers on Be specimens exposed to the DIII-D divertor plasma. The experiments were done with the DiMES probe that held a carbon substrate upon which 100 nm thick films of Be and W were deposited. Specimens at a temperature of about 130°C were exposed to 300 eV D ions for fluences ranging from 1.2×10^{23} to 4.2×10^{23} D/m^2. NRA and RBS analyses were used to characterize the plasma-exposed deposits and to measure the deuterium retention in the films. Approximately 2–4 nm thick carbon surface layers were measured on the Be films. As shown previously in Figs. 6 and 7,

because of the thinness of the carbon film, the measured deuterium retention was only comparable to that in a much thicker sample of pure Be under similar plasma or ion exposure conditions, when the comparisons were made on an equivalent energy scale.

The results of these investigations indicate the following concerning mixed-material (Be, C, O) surface layer formation and hydrogen-isotope uptake and retention for plasma- or ion-exposed Be and carbon-coated Be:

1. Mixed-material surface impurity layers are formed on Be during high-flux exposure to a contaminated plasma, with the thickness primarily dependent on the Be temperature and on the impurity concentration in the plasma.
2. For temperatures above 400°C, Be diffuses into carbon overlayers during heating of carbon-coated Be samples in vacuo. At 500°C, the diffusion rate is greater than 65 nm/h. Be_2C is formed at temperatures above approximately 500°C.
3. Hydrogen isotope retention in previously prepared amorphous-C:H(D) layers on Be is significantly reduced by heating to a temperature of 500°C and higher, resulting in the formation of Be_2C and the release of $H_2(D_2)$. One inference is that hydrogen retention is very low in Be_2C at these temperatures.
4. For Be specimens with impurity layers formed during high-flux plasma exposure, deuterium uptake and retention is a function of growth of the impurity layer and of the test temperature. At 500°C, retention is not significantly greater with impurities present than in beryllium with no impurity layer. However, the effect of impurities on retention increases substantially at lower temperatures.
5. Implantation of deuterium into a thermally mixed C–Be layer on Be at 400°C results in deuterium retention that is about 40% higher than that for implantation into pure Be at the same conditions, probably because of retention in graphitic carbon.
6. Additional experiments are required to better quantify the uptake and retention in complex mixed material surface layers, especially for temperatures between 300°C and 500°C.

3.3. Retention in beryllium co-deposited layers

Experiments on the co-deposition or co-implantation of beryllium and deuterium were performed by Causey et al. [25,42,43] using the TPE linear plasma facility to prepare co-deposited samples and by Mayer et al. [16,44] using an ion-beam system to prepare co-deposited samples. Both experiments used NRA and RBS analyses to characterize the co-deposited samples.

In the TPE experiments, co-deposited samples were prepared by collecting Be that was sputtered from a Be target exposed to the TPE plasma. The sputter target was a 5 cm diameter disk of S65-Be and the implanting deuteron energy was 100 eV. Specific conditions of the most recent TPE experiments were as follows. Sputtered beryllium was collected on a heated 5 mm diameter polished silicon disk located 50 mm in front of the beryllium disk and 50 mm from the centerline of the disk. For experiments performed with the silicon collector plates at 100°C, 200°C, and 300°C, the 100 eV deuteron flux was maintained at 3.3×10^{21} D/m^2 s uniformly over the 50 mm diameter sputter disk. For the experiment performed with the catcher plate at 150°C, the particle flux on the sputter disk was tripled to 9.9×10^{21} D/m^2 s. All of the experiments were run for 1 h. The sputter disk was actively cooled, but still reached a temperature of approximately 150°C. During the plasma exposure of the sputter disk, the deuterium pressure in the system was 3.9×10^{-2} Pa. The background pressure in the system was less than 1×10^{-5} Pa and consisted primarily of water vapor.

After the sputter deposition was completed, the samples were removed from the TPE vacuum vessel and characterized using ion-beam and NRA techniques. Quantitative species profiles in the re-deposited layer on the silicon disks were obtained. RBS analysis with a 2.2-MeV incident He^+ ion was performed to profile oxygen in the samples and to check for unexpected impurities. Elastic recoil detection (ERD) was used to depth profile the amounts of beryllium, deuterium, hydrogen, and carbon in the samples. The incident ion used was Si^{+5} at two energies; 24 MeV to measure the hydrogen, and 28 MeV to measure the other elements. All of the samples were analyzed at room temperature and the measurements were performed consecutively in the same chamber under the same vacuum conditions (less than 1×10^{-5} Pa).

Results from the characterization analyses for the most recent TPE experiments [25] are presented in Table 7. The results, presented as a function of sample or collector-plate temperature, identify the measured thickness of the co-deposited layers and the oxygen and deuterium contents expressed relative to the measured Be concentration. The carbon content, not shown in this table, was found to be less than 1.5% for all of the

Table 7
Measurements from tritium co-deposition experiments performed on the Tritium Plasma Experiment at Los Alamos National Laboratory

Catcher plate temperature (°C)	Thickness (nm)	O/Be	D/Be
100	1.2	0.125	0.15
200	1.2	0.125	0.074
300	1.5	0.06	0.02
150	3.2	0.03	0.10

samples, and no other impurities were identified by this analysis.

Comprehensive studies of Be co-deposition have been reported by Mayer et al. [16,44]. Co-deposited samples were prepared in these experiments with a Be sputter source/collector arrangement that was similar to the Causey experiments [25]. In the work by Mayer et al., a Be target was bombarded with a mass-analyzed beam of 4.5 keV D_3^+ (corresponding to 1.5 keV/D) at normal incidence. The target current was about 0.1 mA, with a beam spot diameter of about 6 mm (giving about 6.7×10^{19} D/m^2 s). A Si-collector placed at a distance of 25 mm from the target at a scattering angle of about 160° was used to collect co-deposited samples. The pressure in the target chamber was about 1×10^{-5} Pa during the deposition experiments. Each co-deposited sample was analyzed using ion-beam techniques. Deposited deuterium was measured with the D(^{3}He,p)α nuclear reaction at 790 keV. Carbon was measured in the deposit using proton enhanced scattering (PES) at an angle of 165°. Deposited beryllium and oxygen were measured via 1.65 MeV proton backscattering at an angle of 165°. To obtain a depth distribution of the co-deposited deuterium, ERDA were made using 60 MeV ^{127}I ions. Quantification of the deuterium composition of the co-deposited layers was also made via thermal desorption measurements, with the co-deposited samples subjected to a linear heating ramp of 5°C/s. Specimen temperatures were monitored by an infrared pyrometer. Experiments were conducted for co-deposited samples prepared for different ion exposure times (about an order of magnitude change in integrated fluence) and with the Si-collector at room temperature [16,44] and at elevated temperatures, 200°C, 300°C and 500°C. [16]

Analyses of the Mayer et al. co-deposited layers revealed significant quantities of oxygen and carbon, in addition to beryllium and deuterium. For the specimens prepared at room temperature, O and Be were present in a 1:1 ratio, characteristic of stoichiometric BeO, whereas the D/Be ratio was 0.36 to 0.38 and the C/Be ratio was about 0.15. For the co-deposited layers formed at elevated temperatures, the quantity of deuterium retained in the layer varied. Ratios of D/Be for the elevated temperature cases were: 0.32 at 200°C, 0.17 at 300°C, and 0.07 at 500°C. Thermal desorption measurements for the co-deposited samples revealed that deuterium release began at 127°C and was essentially complete at 527°C, results that are consistent with TDS measurements by Moller et al. [23] for BeO implanted with energetic deuterium ions.

Mayer et al. [16,44] postulated the following mechanisms to account for the composition of the co-deposited layers formed in their experiments. Co-deposition of deuterium with Be can be understood as an implantation of deuterium into a growing BeO layer. The BeO layer forms via reactions of Be with the vacuum chamber residual gases, H_2O and CO, and grows with increasing deposition and reaction of the sputtered Be. Incorporation of deuterium into the growing BeO layer is caused by implantation of the energetic deuterons that are reflected from the Be target with several hundred eV. Hence, the authors refer to co-deposition of hydrogen with beryllium as co-implantation. Carbon incorporation follows from the Be–CO reaction.

A comparison of the results of the co-deposition experiments for deuterium and Be is given in Fig. 9. In this figure the ratios of hydrogen isotopes to Be are plotted as a function of sample or collector-plate temperature. This figure shows the results from the most recent TPE experiments [25], the earlier TPE experiments [42,43], and the results from Mayer et al. [16,44]. Indications of the relative carbon and oxygen content in the co-deposited layers are noted by each experimental data set. We observe that the most recent TPE results for deuterium retention in co-deposited layers are lower than either of the earlier data sets. We further note that deuterium retention increases in the layers as the oxygen and carbon impurity content increases. The differences in the deuterium, oxygen and carbon contents are most likely related to different experimental conditions during the formation of the co-deposited layers in the various experiments. Experimental conditions that are most important here include the following: (1) the residual gas composition (especially H_2O and CO) and pressure in the vacuum chamber during deposition, (2) magnitude and energy of the deuterium fluxes reflected from the Be targets, (3) magnitude of the Be fluxes sputtered from the Be target, and (4) impurity specifications for the Be

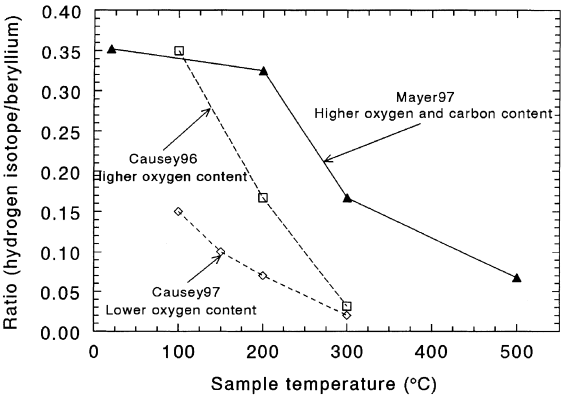

Fig. 9. Comparison of hydrogen isotope contents in different redeposited beryllium films produced by collecting sputtered Be from plasma and ion-beam exposed Be targets. Data correspond to experiments with the TPE simulator (Causey96 [42,43], Causey97 [24]) and experiments with an ion beam (Mayer97 [16,44]). Hydrogen isotope concentrations were measured using NRA, and impurity concentrations were measured using proton backscattering analyses.

targets. Causey noted that the vacuum quality (H_2O partial pressure) improved in the most recent experiments [25] relative to the earlier experiments [42,43] and that this could account for the much lower oxygen and deuterium retention in the sputter-deposited Be layer. Based on the reported vacuum conditions for the recent Causey experiments [25] and the Mayer et al. experiments [16,44], the H_2O and CO partial pressures may be comparable for the two experiment sets. Yet, the O and C impurity content in the co-deposited layers is much higher in the Mayer experiments. This could be due to differences in the magnitudes of the deuterium and Be fluxes incident on the collector, relative to the fluxes of residual gas H_2O and CO that are incident on the collector. For the Mayer experiments, taking into account the deuterium flux incident on the target, the D reflection coefficient and the Be sputter coefficient for 1.5 keV D, and the residual gas pressures, the reflected D and sputtered Be fluxes impinging on the collector are comparable to one another and to the arrival fluxes for residual H_2O and CO. Consequently, a BeO layer grows and incorporates C and energetically-implanted D as the deposition continues. Based on the TDS data, Mayer et al. [16] postulate that the deuterium is not associated with gas bubbles and blisters but is trapped at defect sites in the BeO. In contrast, for the Causey experiments, the plasma flux incident on the Be target is about two orders of magnitude greater than the implantation flux of the Mayer experiments. Taking into consideration the deuterium flux incident on the target, the D reflection coefficient and the Be sputter coefficient for 100 eV D, and the residual gas pressures, the reflected D and sputtered Be fluxes impinging on the TPE collector are about two orders of magnitude greater than the arrival fluxes for residual H_2O and CO. Consequently, the sputter-deposited Be layer grows with much lower C and O impurities. Furthermore, the reflected deuterium from the TPE Be target has an average energy of 30 eV [25], so implantation into the depositing Be is very shallow and the implanting particles produce little if any displacement damage in the Be layer. Consequently, deuterium incorporation into the co-deposits prepared with TPE is substantially lower than that in the co-deposits prepared by Mayer.

In support of Mayer's conclusion that codeposited hydrogen isotopes may be trapped at defect sites in BeO layers, Alimov et al. [45] have recently analyzed deuterium implanted into BeO. The oxide was carefully grown on polished Be to a depth of about 120 nm. Deuterium at 3 keV was implanted to a depth of 37 ± 12 nm with the target at room temperature and 427°C. A combination of SIMS, RGA and TEM analyses revealed that saturation in the BeO layer occurred at 1.8×10^{21} D/m^2 for the 27°C samples and at 0.7×10^{21} D/m^2 for the 427°C samples. The deuterium was found to be in both the atomic and molecular forms with the molecules resident in tiny bubbles (0.6–0.7 nm radius, 4.5×10^{22} m^{-3} concentration) and in intercrystalline gaps. The ratio of atomic to molecular D was 8:1 for the room temperature implantation and 2.5:1 for the 427°C tests. Most of the atomic D appeared to be in lattice point defects.

Even the recent TPE results are higher than concentrations predicted by the DIFFUSE [46] computer code. While these experiments are identified as co-deposition experiments, the re-deposited beryllium layers are in fact constantly bombarded with deuterons reflected from the sputter source. The flux of these reflected particles onto the re-deposited layers is approximately 1.4×10^{20} D/m^2 s (three times this value for the layer produced at 150°C). The average energy of the reflected particles is 30 eV. Based on DIFFUSE calculations for these flux and energy conditions, the predicted deuterium concentrations in a Be layer are very much less than the measured values. Scanning electron microscopy analyses for the samples provided a clue to resolving this discrepancy. The lower temperature exposed samples were found to contain deuterium bubbles and blisters. The existence of these bubbles and blisters is consistent with shallow implantation of deuterium with energies less than the damage threshold, and it provides additional evidence that the solubility of hydrogen isotopes in pure beryllium is very nearly zero.

The results of these investigations indicate the following concerning co-deposition of hydrogen with Be.

1. Hydrogen isotope retention in re-depositing Be is very dependent on the relative magnitudes of the hydrogen and beryllium fluxes and the fluxes of oxygen and carbon that are incident on the collecting surface and on the energy of the incident hydrogen.
2. If the oxygen and carbon impurity fluxes are comparable to the hydrogen and beryllium fluxes, the re-depositing Be layer will most likely grow as a BeO layer with incorporated carbon. If the hydrogen is energetic enough to be implanted in the BeO layer and cause displacement damage, it will be retained at the damage sites. Retention will saturate at a D/Be ratio of about 0.35 if the temperature is at 100°C or below.
3. If the oxygen and carbon impurity fluxes are significantly less than the hydrogen and beryllium fluxes, the re-depositing layer will most likely be relatively pure Be with low oxygen and carbon impurities. Hydrogen retention will be low and dependent on the formation of near surface bubbles and blisters.
4. Temperatures above 527°C are sufficient to remove retained hydrogen from co-deposited BeO/C layers formed with energetic (hundreds of eV) hydrogen.
5. Retention of hydrogen in re-deposited Be with low oxygen and carbon impurities approaches zero for temperatures above 300°C.
6. Experiments are required to investigate hydrogen uptake and retention in re-deposited Be layers with high

oxygen and carbon impurities when the incident hydrogen particles have energies below the damage generation threshold for Be and BeO.

3.4. Microstructural evolution in hydrogen-implanted beryllium

Many experimental investigations have provided evidence for significant microstructural modification of beryllium that is implanted with energetic hydrogen ions. In some studies, a variety of techniques including optical microscopy, SEM, TEM, and positron-beam depth profile analyses have been used to examine and characterize the microstructure of ion-implanted materials. Micro-chemical characterization of the beam-modified zone in ion-implanted Be has been accomplished by Auger spectrometry and by various ion-beam analysis techniques such as RBS and NRA. In many cases the relationship between microstructural modification and hydrogen retention was also explored by further experiments and analyses of implanted specimens. These experiments entailed primarily thermal desorption studies and ion-beam analyses such as ERDA and NRA for implanted specimens to determine the quantities of retained hydrogen or deuterium. A summary of the salient features of these experimental studies is provided in the following paragraphs.

Early studies on hydrogen ion-bombarded Be were reported by Verbeek and Eckstein [47], by Liu et al. [48] and by Langley [14]. Verbeek and Eckstein observed blister formation on the surface of beryllium that was exposed at room temperature to 15-keV D^+ ions at fluences of 3×10^{21} D/m^2 or greater. SEM analyses showed blisters with diameters of a few μm, some of which were ruptured. Liu et al. investigated trapping of deuterium in Be exposed at room temperature to 10 keV D^+ ions to a fluence of 1.5×10^{23} D/m^2. Although, these authors did not characterize the beam-modified surfaces, they measured the retained quantities of deuterium by a thermal desorption technique. Because the measured retained quantities were two orders of magnitude greater than the quantity estimated from solubility considerations, these authors concluded that the retained quantities could only be accounted for by retention in intact blisters or by trapping as sub-microscopic bubbles or at radiation damage sites. Interestingly, in the studies by Langley, who implanted room-temperature Be with 5 keV diatomic deuterium to fluences of 1×10^{23} D/m^2, no blister formation was observed. However, Langley did observe a significant growth of a BeO layer in the beam-exposed region of the sample.

Some later studies that specifically explored the retention of deuterium in ion-implanted Be were reported by Wampler [18,33] and by Kawamura et al. [49]. In the earlier work by Wampler [18], high-purity CPM Be specimens were implanted at room temperature with 0.5 and 1.5 keV D^+ ions to fluences that varied from 1×10^{20} D/m^2 to 5×10^{21} D/m^2. Retention as a function of fluence was measured using NRA. A saturation concentration of 0.31 D/Be was deduced from the NRA analyses. Dips were observed in the 1.5 keV retention data at high fluences, indicating the possible influence of blister formation and cracking, phenomena that were confirmed by SEM analyses that revealed 0.4 μm diameter blister domes on the surface. Thermal desorption measurements by Wampler [18] indicated that retained deuterium was released in two stages, a broad stage at 400 ± 100°C and one at 125°C. For samples implanted to saturation, most of the retained D was released in the 125°C stage but no release occurred at this temperature for low dose implants. Wampler postulated that implanted deuterium most likely precipitated into bubbles or was bound to ion-induced traps in the implantation zone of the Be. Deuterium retention in this study was consistent with that reported by Liu et al. [48] but much less than that reported by Langley [14] who most likely observed hydrogen retention in a growing BeO layer rather than in Be. A more extensive study of trapping mechanisms was reported in a later paper by Wampler [33] in which ion-beam techniques were used to study de-trapping and thermal release of deuterium implanted into single crystal Be samples at room temperature. These studies revealed that at low concentrations (<0.01 D/Be) the implanted D is trapped at lattice damage from its own implantation, and de-trapping occurs around 450°C. At high concentrations ($\gg 0.01$ D/Be), D precipitates into gas bubbles prior to release at temperatures higher than 450°C. Kawamura et al. [49] reported the results of retention studies in which CPM Be samples were implanted at room temperature with 5 keV D_2^+ ions to fluences that varied from 5×10^{21} D/m^2 to 7.3×10^{22} D/m^2. Deuterium concentrations in the implanted Be were measured with ERD using 1.5 MeV He^+ ions and oxygen impurities were measured by RBS. SEM analyses revealed the presence of 0.5 μm diameter blisters on the implanted Be surface. These authors observed a saturation concentration thermal release behavior consistent with that of Wampler [18].

Surface material modifications have been studied in some detail by Anderl et al. [35,50,51] for high-purity CPM Be and ingot metallurgy Be foils that were implanted at room temperature and at temperatures around 400°C. Although the emphasis of the first experiments [35] was on measuring permeation associated with implantation of 1 keV D onto specimens heated to temperatures from 420°C to 450°C, post-implantation analyses for the specimens revealed a significantly modified microstructure in the implantation zone. Because the permeation experiments were conducted to high-implantation fluences (2×10^{24} D/m^2), sputter erosion of the surface uncovered the deep modified

microstructure permitting detailed SEM characterization of its features. SEM analyses revealed that the implantation zone exhibited a highly porous structure of cavities (1 μm or less in diameter) that were interconnected to cavities deeper into the material. For the ingot metallurgy material, some of the cavities had a hexagonal cross-section that corresponded to the hexagonal-closed-packed (hcp) structure for Be. SEM analyses of a cross-section through the implantation zone revealed that the modified structure was about 1 μm deep, significantly deeper than the implantation range of 16 nm for the implanting deuterium. NRA measurements were made of the implantation zone using an 800 keV $^3He^+$ beam to determine the deuterium concentration indicating that the retained deuterium concentration reached a maximum of about 0.1% at a depth of 0.2–0.4 μm. These characterization studies provide evidence that thermal transport and agglomeration of beam-induced vacancies beyond the implantation range, as well as deuterium trapping at vacancy complexes and deuterium precipitation, result in significant void growth and bubble generation in Be that is implanted with deuterium to high fluences at temperatures near 400°C.

The results reported by Anderl et al. [50,51] extended the previous characterization studies [35] for deuterium-implanted Be by including the following: (1) implantation of unannealed and annealed Be foils at room temperature and at temperatures near 400°C, (2) implantation with ion beams of varying energy (300 eV to 1 keV D), (3) microstructural characterization using SEM and positron-beam depth profile analyses, and (4) micro-chemical characterization using depth-profile Auger analyses. SEM analyses revealed that the high-temperature implantations resulted in a modified surface structure like that described in the previous paragraph, whereas implantation of Be at room temperature resulted in blister formation. Depth-profile Auger analyses revealed that growth of a BeO layer in the implantation region was highly dependent on the specimen temperature and on the energy and flux of the implanting deuterium ions. Oxide growth, resulting from interaction of surface Be atoms with residual background gases, is impeded if the ion energy and flux provide high-sputter erosion rates. Oxide growth occurs if the sputter erosion rates cannot compete with oxide formation rates.

Positron-beam depth profile analyses [50,51] identified a varying defect structure in beryllium, dependent on the previous anneal history of the material and on the temperature of the material during implantation with energetic deuterium ions. For specimens implanted at room temperature with 1 keV/D ions, the beam-induced defect structure had a profile that was peaked near the mean range of the implanting deuterium and that extended beyond the implantation zone. Isochronal step-thermal anneal experiments revealed that deuterium was released from these defects at a temperature of about 125°C, indicative of shallow traps, and that the defects annealed at temperatures above 300°C, results that correlate well with the thermal desorption measurements by Wampler. [18] The positron studies indicated that, for Be implanted at room temperature with 1 keV D, the beam-induced vacancy–defect complexes were most likely 1 nm voids. For beryllium implanted at temperatures of 450°C with 1 keV/D ions, positron-beam depth-profile measurements revealed a different defect structure than that for specimens implanted at room temperature. In this case, the beam-induced defect structure was much broader and extended far beyond the implantation zone. Isochronal step-thermal anneal experiments for these specimens revealed a more stable defect structure, with the onset of defect annealing at 500°C. There was no evidence of deuterium release at lower temperatures, indicating that for beryllium implanted at elevated temperatures, deuterium is retained in deep traps. These measurements indicated that, for beryllium implanted at 400°C, beam-induced defects most likely consist of large stable voids with defect concentrations less than that for material implanted at room temperature.

Touche and Terreault [52] have reported the results of an extensive characterization study for deuterium ion-implanted Be that is similar to the work of Anderl et al. [35,50,51] Using SEM analyses to characterize the surface microstructure of beryllium implanted with 1.5 keV deuterium ions with fluences ranging from 3×10^{20} to 1.2×10^{22} D/m^2 and specimen temperatures ranging from 20°C to 710°C, these researchers observed that, for specimens heated to temperatures above 200°C and for fluences greater than 1.8×10^{21} D/m^2 (saturation fluence), blisters were created that were larger than at lower temperature implants, and they were interconnected. For temperatures below 200°C, the surface structure exhibited smaller blisters that were not ruptured.

3.5. Effects of neutrons

Neutrons are known to produce a number of effects in beryllium. These include gas production, swelling, and changes in microstructure. When considering tritium retention and release in beryllium, these neutron-induced processes must be considered.

Neutrons from the an ITER-like plasma will cause transmutations in beryllium that will result in tritium production. It is important to be able to properly account for this source of tritium when estimating tritium inventory and permeation in an ITER-like tokamak. One production mechanism occurs as the following reactions take place:

$$\begin{aligned} &^9\mathrm{Be} + n \rightarrow {}^6\mathrm{He} + {}^4\mathrm{He} \\ &^6\mathrm{He} \rightarrow {}^6\mathrm{Li} + \beta^- \\ &^6\mathrm{Li} + n \rightarrow {}^3\mathrm{H} + {}^4\mathrm{He}. \end{aligned} \quad (1)$$

The two-step nature of this reaction (the ^{6}He decay is almost instantaneous) is an indication that the production of tritium will not scale linearly with neutron fluence. Another major mechanism is the pathway:

$$^9\mathrm{Be}+n \rightarrow {}^7\mathrm{Li}+{}^3\mathrm{H}$$
$$^7\mathrm{Li}+n \rightarrow {}^4\mathrm{He}+{}^3\mathrm{H}+n'. \quad (2)$$

Forty et al. [53] calculated tritium production in beryllium for a representative fusion environment using the FISPACT code. They determined that about 64% of the tritium production came through the pathway of Eq. (1) and 33% came through that of Eq. (2). The remaining 3% was produced by alternate reaction pathways considered in their analysis. Their results for tritium inventory, I (appm), as a function of the total neutron fluence, ϕt (MWa/m^2) are reasonably fit by the equation [54]

$$I(\mathrm{appm}) = 280\phi t - 2350[1 - \exp(-0.1\phi t)]. \quad (3)$$

In addition to tritium production, neutron irradiation produces even larger amounts of helium and defects in the beryllium structure.

Stepped-isothermal anneal experiments were conducted at the INEEL to investigate tritium and helium release behavior from beryllium irradiated to a fast neutron fluence of 5×10^{26} n/m^2 in the Advanced Test Reactor (ATR) [55]. The beryllium test specimens were of the same type used in the initial ATR construction. Irradiation was at 75°C. In-line ion-chambers and on-line quadrupole mass spectrometers were used for simultaneous analysis of the released gas concentrations in an Ar process stream flowing over the heated specimens.

Two experiments were conducted in which the temperature was varied from room temperature to high temperatures in several steps. In one experiment in which 200°C temperature steps were taken from 200°C to 1000°C, greater than 99.8% of the available tritium and 52% of the helium (^{3}He and ^{4}He) were released in the step from 600°C to 800°C. The remaining helium was released in the step from 800°C to 1000°C. In contrast, for the other experiment in which a Be specimen was heated in 50°C steps from 600°C to 800°C, followed by a 200°C step to 1000°C, 86.3% of the available tritium was released with the specimen at 650°C. For this experiment, 71% of the available helium was released in the step to 1000°C and higher, indicating that only about 29% of the helium was released during sample heating at 650°C. In both cases the major gas release occurred as a 'burst'; however, the maximum release rate was much smaller in the second experiment than in the first.

The time dependence of the gas-release rates was much different between the two experiments, with the release rates falling off much faster in the first experiment than in the second. Researchers observed concurrent release of tritium and helium gases during the major release events for both experiments, providing direct evidence of these gases in helium bubbles in the irradiated beryllium. A quantitative analysis of the gases released during the 800°C step in the first experiment gave the following relative gas composition: 6% H_2, 7% ^{3}He, 2% HT, 81% ^{4}He, and 4% T_2. The determination of the original inventories of entrapped tritium and helium (^{3}He and ^{4}He) in the Be specimens tested in these experiments are in good agreement with the measurements reported by Baldwin et al. [56,57] and by Beeston et al. on specimens from the same lot, [32] provided one takes into consideration the decay of tritium between the various tests.

Additional INEEL experiments were performed on fully dense beryllium cylinders irradiated in the EBR-II reactor to a fast neutron ($E > 0.1$ MeV) fluence of 6×10^{26} n/m^2 [58]. Prepared from Brush Wellman S200-E powder, the samples were cold isostatically pressed, sintered and then hot isostatically pressed. The nominal irradiation temperature was 400°C. Following irradiation, the samples were annealed at temperatures from 450°C to 1200°C. The releases of tritium and helium were measured during the heat-up phase and during the high-temperature anneals. These experiments revealed that at 600°C and below, there was insignificant gas release. Tritium release at 700°C exhibited a delayed increase in the release rate. For anneal temperatures of 800°C and higher, tritium and helium release was concurrent, and the release behavior was characterized by gas-burst peaks. Essentially all of the tritium and helium were released at temperatures of 1000°C and higher whereas about one tenth of the tritium was released during the anneals at 700°C and 800°C. Subsequent specific surface area measurements revealed that annealing of irradiated beryllium caused a porosity network to evolve and become surface-connected to relieve internal gas pressure.

Previously, Baldwin et al. [56] and Baldwin and Billone [57] had performed similar stepped annealing experiments on samples irradiated in the ATR. Two of the samples (81% and 99% theoretical density, 2.6×10^{25} n/m^2, $E > 1$ MeV) were from the same fabrication lot as the EBR-II specimens mentioned above, while the 100% dense sample was from the same lot as the ATR original construction specimen (5×10^{26} n/m^2, $E > 1$ MeV). They monitored the tritium evolving from the specimens as temperatures were increased, usually in 100°C increments, from 300°C. For the fully dense material, they observed a burst release at about 611°C, similar to the one seen in the INEEL experiments just mentioned. Less than 1% of the total tritium had come out at lower temperatures with an apparent activation energy of about 0.8 eV. Results for the lower fluence 99% dense sample were similar except that about 20% of the available tritium was released before the burst took

place. For the 81% dense sample, about 80% of the tritium had evolved before the sample had reached 600°C. Baldwin and Billone [57] showed that the time variation of tritium evolution from the samples was well fit by a diffusive model with different diffusivities for the various densities of material. Longhurst [54] subsequently showed that the same data could be fit using the Abramov diffusivity for high-purity beryllium [59] and appropriate combinations of trap concentration and trap energy.

It is evident that tritium retention and release in neutron-irradiated beryllium is a complex function of material density as well as neutron fluence and energies and irradiation temperature. The ANFIBE code [60,61] developed at Forschungszentrum Karlsruhe is reasonably successful in simulating the production and swelling phenomena associated with neutronic transmutations. However, it has not yet been made generally available, and it remains to be confirmed under the full range of fusion operating conditions. Substantially more data are required on neutron-irradiated material to fully understand these effects, particularly the trapping effects due to gas production and displacements.

4. Models for predicting tritium retention in Be PFC materials

Conventional wisdom, applicable in a wide variety of experiments, has been that hydrogenic atoms or ions implanting into a metal will diffuse both ways from the implantation zone. Atoms that reach the surface may recombine with other diffusing hydrogenic species or with receptor atoms such as oxygen present on the surface to form molecules that are then released to the gaseous state above the surface [8]. Traps present in the material can retard diffusion and enhance retention of the hydrogenic atoms during a thermal transient. Recent experiments at high fluxes have indicated hydrogenic atom retentions that are well below that predicted by the diffusion/recombination model, exhibiting a saturation effect. In this section we consider models in both regimes and show how they fit experimental data.

4.1. Conventional diffusion/recombination model

TMAP4 [62] is a versatile code for modeling processes of implantation, retention and re-emission of tritium from materials though others, such as DIFFUSE [46] and PIDAT [63] to name two, have also been developed using the same general approach. Other codes such as BETTY [64] and ANFIBE [65] while using the same transport equations have approached the problem in a more complex way. These codes are based on theory, which is well summarized by Walbroeck et al. [8] Experiments conducted in the laboratory at low fluxes where saturation is not evident suggested that tritium inventories in ITER could be calculated assuming a diffusivity given by Abramov [59], solubility given by Shapovalov and Dukel'ski [66], recombination given by Hsu [67] and subsequently modified by Andrew [68] and then by Causey [69]. Such calculations have been performed and reported [70,71].

4.2. Saturation model

When ion fluxes to the surface are high, hydrogen concentration saturates in the implantation zone. Observations from the experiments described in Section 3 regarding hydrogen ion saturation in beryllium include the following points.

1. Especially at high fluxes, there is a temperature-dependent saturation concentration in beryllium that appears not to be exceeded. This limits the driving potential for diffusion of hydrogen isotopes into the bulk of the material and thus limits inventories that may develop.
2. Injected gas precipitates into bubbles nucleating at grain boundaries and defect sites. Gas pressure in the bubbles is very close to equilibrium with surface tension when the bubbles are small [20] but as the bubbles become larger and connected porosity develops, the pressure appears to reduce to something near metal yield strength [72].
3. The development of surface connected porosity results in a substantial increase in surface area through which implanted hydrogenic atoms can emerge. This leads to an increase in effective recombination coefficient and in effective diffusivity in the implantation zone.
4. There is a damage region much deeper than the implantation zone where traps are more numerous than they are in the bulk of the beryllium [35]. The extent of this region appears to correlate with implanting ion energy, but it is also strongly temperature dependent, increasing with increasing temperature.
5. Depending on ion flux and plasma composition, an oxide, carbide, or other impurity film may form on the plasma-facing surface at all operating pressures. There may even be an oxide film at the surface of carbon coatings on Be [73]. In many experiments involving hydrogen transport in beryllium, the rate limiting processes are associated with surface films [74]. This does not appear to be controlling when saturation is active.
6. At the high-ion fluxes of the TPE and PISCES experiments and in ITER baffles, surface erosion will be substantial and must be taken into account in modeling.

These observations provide the motivation and basis for the mathematical model that has been developed to

simulate saturation of implanted hydrogen in beryllium. The model specifically addresses enhanced recombination, enhanced diffusion, erosion and trapping. The total flux of mobile hydrogen ions to the surface is

$$J_i = -\left(2K_r n_{i_0}^2 + u n_{i_0}\right), \tag{4}$$

where K_r is the recombination coefficient, n_{i_0} the mobile atom concentration at the surface, and u represents the erosion face velocity. The negative sign indicates that the recombination current is in the negative x direction for positive u. The erosion velocity is taken to be the product of particle arrival rate and the sputtering yield for the ion–material pair. Accounting for erosion is important in high-flux situations where return to the plasma of hydrogen atoms in the lattice by erosion is significant compared with diffusional transport.

As the surface of the material becomes saturated with implanted hydrogen atoms, those atoms that cannot be carried away by diffusion must precipitate in bubbles or collect at defects. A channel must be opened for their rapid return to the plasma, effectively enhancing the rates of recombination and diffusion between the implantation depth and the surface.

A change in K_r can be made to partially accommodate the increased release rate for implanted atoms that is typical of saturation effects. This is accomplished by allowing the recombination coefficient to grow exponentially when the surface concentration reaches the saturation level. A very high recombination rate will produce what amounts to a zero-concentration boundary condition once it becomes activated. The resulting equation for K_r is

$$K_r\left(\frac{m^4}{s}\right) = \left[3.4\times 10^{-29}\exp\left(\frac{-0.28\text{ eV}}{kT}\right)\right] \times\left[1+\exp\left(\frac{10 n_{i_0}}{n_{\text{sat}}}-10\right)\right]+\frac{u}{1+n_{i_0}}. \tag{5}$$

Here the first term in brackets is the Hsu–Andrew–Causey [67–69] value for the recombination coefficient for deuterium on beryllium obtained at low fluxes. It is important that this function is retained for short-term response under ITER-like conditions or for low-flux operation. The term in the second set of brackets accomplishes the exponential growth at saturation, and the last term accommodates loss of hydrogen from the surface by surface erosion. The factor of 10 used inside the exponential, the acceleration factor, is somewhat arbitrary provided it is sufficiently large. Again, the term n_{i_0} is the surface mobile atom concentration of species i, while n_{sat} is the product of the square root of material yield stress (Sieverts' law with equilibrium pressure equal to the yield stress) and Shapovalov and Dukel'ski [66] solubility. The result is evaluated from

$$n_{\text{sat}}\left(\frac{\text{atom}}{m^3}\right) = \frac{4.079\times 10^{26}}{\left[1+0.0012\ T+\left(\frac{T}{950}\right)^{16}\right]^{1/2}} \times\exp\left(\frac{-0.17\text{ eV}}{kT}\right). \tag{6}$$

The diffusivity in the region between the implantation depth and the surface must be enhanced to complete the representation of the rapid release of implanted atoms under saturation conditions. This is modeled by multiplying the diffusivity in the surface region by the same enhancement factor as appears in Eq. (5).

The temporal development of hydrogenic ion inventories and permeation rates may be handled in one of two ways. The actual temporal variation in ion and heat loadings to the surfaces may be included by suitable equations that may make use of ramps, unit step functions, etc. and the calculation continued over the full period of tokamak operation. As an alternative, the periods of activity when the plasma is present may be simply concatenated, eliminating the dormant periods between plasma pulses. The success of the latter approach is contingent on diffusion, trapping, and release all undergoing substantial arrest when the temperatures of the structures drop between pulses. For beryllium structures operating at 100–400°C, that will generally be the case.

4.3. Application of models

Application of the above discussed modeling technique has given excellent agreement when applied to experiments conducted in the laboratory [13]. Most of the early experiments such as those of Hsu [67] and Saibene et al. [75] were run under low ion fluxes and to modest fluences such that the saturation effects were not evident. Nevertheless, results using this model gave excellent agreement with measurements. Fig. 10 compares the measured data of Hsu with a TMAP4 calculation using saturation theory. The 1/t correlation is Hsu's. Efforts to simulate more recent experiments such as those of Causey on TPE [24] where saturation effects are clearly evident have also been highly successful [13] as shown in Fig. 11. Neglecting the erosion effect in calculations replicating TPE experiments resulted in an overestimation of tritium/deuterium retention by a factor of 3.

A further calculation was made to replicate results of experiments performed by Doerner and Wampler [76] in which beryllium samples were exposed to intense plasmas on the PISCES-B facility and then examined by NRA and by TDS. These experiments were discussed in Section 3.1 above. Taking the same model used for the TPE simulations, calculations were performed on 1.6 mm thick beryllium specimens exposed to 100 eV deuterium ions at fluxes of 1.5×10^{21} D/m^2 s for the 200°C

Table 8
Comparison of experimental measurements of deuterium retention in 1.6 mm thick beryllium samples exposed to 100 eV ions in PISCES-B with calculations simulating those experiments using the TMAP4 code (NRA measurements were effective down to about 6 μm whereas TDS measurements measure the total inventory of the specimens)

Temp (°C)	Flux (D/m^2 s)	Fluence (D/m^2)	Experiment		Calculation	
			NRA (D/m^2)	TDS (D/m^2)	6 μm inv. (D/m^2)	Total inv. (D/m^2)
200	2.7×10^{20}	2.7×10^{20}		2.7×10^{20}		
		1.1×10^{21}	2.5×10^{20}	6.3×10^{20}	4.5×10^{20}	6.9×10^{20}
		4.3×10^{21}		3.6×10^{20}		
500	9.0×10^{21}	2.9×10^{21}		2.1×10^{20}		
		6.5×10^{21}	6.6×10^{19}		2.2×10^{20}	6.0×10^{20}
		1.2×10^{22}		2.1×10^{20}		
		3.5×10^{22}		2.6×10^{20}		

test and 9.0×10^{21} D/m^2 s for the 500°C test, respectively. NRA measurements are shown in Fig. 8. In Table 8, those and similar measurements are compared with TDS measurements on similar samples. Also shown are the results of the TMAP4 calculations for the same quantities. Calculations were only performed for those experiments where NRA measurements were available. Inventory over the first 6 μm of sample depth should correspond with NRA measurements, and total inventory should correspond with TDS data. Agreement is reasonably good considering that the actual experimental samples were coated with oxides, as previously discussed, and possibly carbides. These have an effect on retention that is not included in the model used.

With that success as a basis, we undertook the estimation of tritium inventories and permeation in the Be-clad FW of ITER during the BPP. Erosion was included in the modeling, not so much for the removal rate of tritium from the surface but for the long-term reduction in thickness of the surfaces, thus reducing inventory. The key parameters for the FW are in the first row of Table 2. The higher particle flux of 10^{20} D + T/m^2s was assumed. Results for inventories are given in Fig. 12. The calculated permeation was an exponentially rising function in each case. For conventional recombination-limited calculations the maximum value at the end of the BPP was 0.2 g/day (calendar day, not plasma-on time). When saturation and erosion were included in the model, using the same combination of parameters that were used to fit the TPE experimental data in Fig. 11, the permeation rate at the end of the BPP through the FW was only 0.7 mg/day. Comparing the inventory results for the conventional recombination-limited model with calculations implementing saturation and erosion in Fig. 12, as well as tritium breeding from the neutrons, the recombination model estimated an inventory of 801 g at the end of the BPP as compared with 106 g when saturation and erosion were considered. The significance

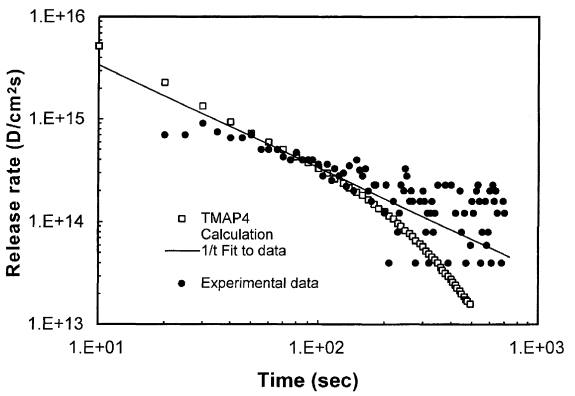

Fig. 10. Calculation of deuterium release in the experiment of Hsu [67] using saturation and erosion in the TMAP4 code even though they are not significant under the conditions of the experiment.

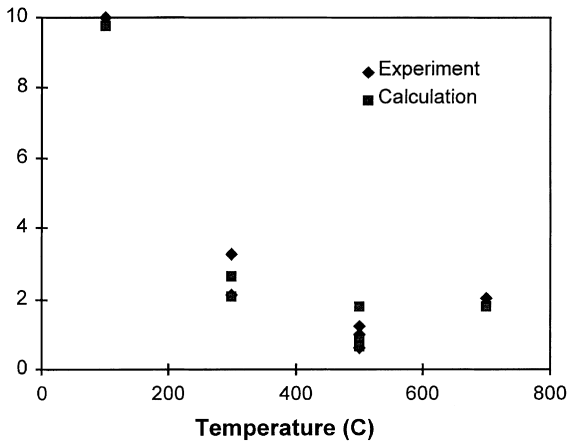

Fig. 11. TMAP4 with saturation and erosion gave excellent agreement with measurements of deuterium retention in beryllium in the Tritium Plasma Experiment [24]. Plasma ion currents ranged from 0.8 to 9 amp into the 5 cm diameter beryllium test specimens held at the various temperatures shown. The insensitivity to ion flux demonstrates the saturation process.

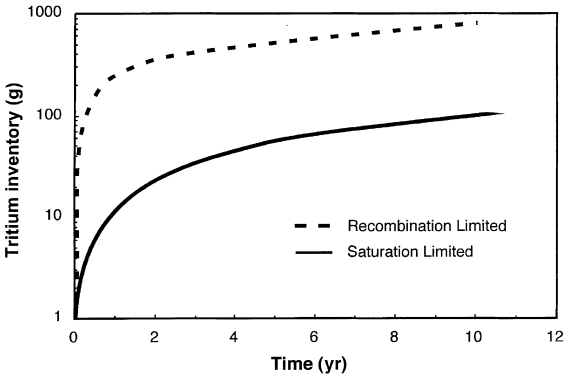

Fig. 12. Comparison of predictions for ITER first wall inventory under saturation and recombination-limited recycling to the plasma assumptions.

of including the saturation and erosion processes in the calculations for pure beryllium is obvious. Additional work is needed to quantify the effects of surface impurities on these processes.

5. Discussion and conclusions

The experimental data reviewed here clearly show the following

1. Under ITER-like implantation conditions ($>10^{20}$ D + T/m^2 s, $E > 100$ eV), hydrogenic atom concentrations saturate near the surface of beryllium causing damage and resulting in strongly enhanced rate of return of plasma ions and atoms to the surface.
2. The quantity of hydrogenic atoms retained in the near-surface region (well beyond the implantation depth) is dependent on the temperature of the specimen and to a lesser extent on the energy of the implanting ions.
3. Less hydrogen is retained at elevated temperatures than at lower ones; and inherent porosity, such as in plasma-sprayed or in less than fully dense beryllium, also reduces the amount retained. Retention is not very dependent on the impinging particle fluence.
4. When saturation takes place, the amount of tritium or other hydrogenic species diffusing deep into the beryllium is reduced compared with that in circumstances where saturation does not occur.
5. In experiments where ion fluxes are much lower, more conventional processes of recombination-limited return of plasma particles to the surface seem to dominate.
6. Hydrogen species appear both in the atomic and in molecular forms in the near-surface region. In both the bare metal and in oxide-coated surfaces, the molecular gas seems to be associated with bubbles, small or large depending on the thermal history of the material. Atomic hydrogen may be resident, attached to impurities or in crystalline defects.

New results on the co-deposition or co-implantation of beryllium and deuterium are now available from various laboratories and were presented here. The results of these investigations indicate that:

1. Hydrogen-isotope retention in re-depositing beryllium is very dependent on the relative magnitudes of the hydrogen and beryllium fluxes and the fluxes of oxygen and carbon that are incident on the collecting surface, as well as on the energy of the incident hydrogen.
2. If the oxygen and carbon impurity fluxes are comparable to the hydrogen and beryllium fluxes, the re-depositing beryllium layer will probably grow as a BeO layer with incorporated carbon and hydrogen.
3. If the hydrogen is energetic enough to be implanted in the BeO layer and cause displacement damage, it will be retained at the damage sites.
4. If the oxygen and carbon impurity fluxes are significantly less than the hydrogen and beryllium fluxes, the re-depositing layer will probably be relatively pure Be with low oxygen and carbon impurities. Hydrogen retention will be low and dependent on the formation of near-surface bubbles and blisters.
5. Temperatures above 500°C are needed to remove retained hydrogen from co-deposited BeO/C layers formed with energetic (hundreds of eV) hydrogen. Retention of hydrogen in re-deposited Be with low oxygen and carbon impurities approaches zero for temperatures above 300°C.

In conclusion, the estimate of tritium retention in re-deposited Be for ITER is highly dependent on the knowledge of the oxygen and impurity fluxes incident on the collecting surfaces, and this was accounted for in recent calculations [77,78].

The amount of carbon or oxygen on the surface of plasma-exposed beryllium depends on the relationship between the content of those species in the plasma and the flux and sputter efficiency of the hydrogenic ions. Carbon and oxygen coatings on beryllium have an influence on retention and release of hydrogen in the substrate. If the temperature rises high enough, beryllium will diffuse through the surface films to form oxide and/or carbide, and it can liberate hydrogen attached to oxygen and/or carbon in the process.

In modeling retention of deuterium and tritium in plasma-facing surfaces, it is important to include the effects of saturation when they apply. Predictions for tritium retention in ITER based upon recombination theory give inventories many times those in which saturation is included. The saturation model used with TMAP4 is based on a maximum mobile atom concentration that depends on material yield strength and hydrogen solubility. Using this technique, recombination and diffusion near the surface are allowed to grow as

large as needed to limit the mobile atom concentration in the beryllium to the saturation value. It gave excellent agreement with experimental results under ITER-like conditions as well as under circumstances where the particle fluxes were lower.

Tritium is produced in beryllium by neutron transmutation reactions. The amount produced and the ratio of tritium to helium produced depend on the neutron fluence and energy spectrum. Gas production characteristics are reasonably well understood. Additional studies are warranted on the detailed mechanism(s) for retention of tritium in neutron irradiated beryllium.

The present understanding of hydrogen interactions with beryllium surfaces under ion and atom implantation is much more complete than it has previously been, due to the innovative experiments conducted by researchers around the world, largely in support of the ITER Project. However, there are a number of concerns.

1. One key to obtaining good estimates of inventories and uptake/release kinetics is the proper selection of trap energies and concentrations. These are strongly dependent on material fabrication and thermal histories and on the effects of neutrons in transmuting beryllium to helium and tritium and in producing atom displacements. Understanding those effects in a way that will allow a priori determination of trap concentrations and energies is one area that yet requires considerable study.
2. A second important concern, especially for ITER-like plasma conditions, is the adequate determination of the purity of the plasma implanting into the beryllium. While it is estimated that plasma-facing beryllium will be scoured clean of oxygen or carbon buildup, that point needs to be ascertained.
3. Another concern for fusion applications generally is the considerable difference in hydrogen transport properties expected if alloying of the beryllium with aluminum or other metals is considered.

Hence, though the interactions of hydrogenic ions and atoms with beryllium are much better understood than they were, there is yet much to be learned on this important topic.

Acknowledgements

This work was performed for the US Department of Energy, Office of Energy Research under DOE Idaho Operations Office Contract DE-AC07-94ID13223 and under other contracts at the respective institutions of the authors. The authors gratefully acknowledge the many helpful conversations with others active in this area of investigation, both within the US and Canada and in other countries, that have helped to clarify understanding and expand on information available in the literature.

References

[1] K.L. Wilson et al., J. Vac. Sci. Technol. A 8 (3) (1990) 1750.
[2] P.H. Rebut et al., JET-R(85)03, JET Joint Undertaking, Abingdon, Oxfordshire, UK, 1985.
[3] E. Bertolini, Fus. Eng. Des. 27 (1995) 27.
[4] R. Sartori et al., J. Nucl. Mater. 176&177 (1990) 624.
[5] G. Alefeld, J. Völkl (Eds.), Hydrogen in Metals, Basic Properties, Springer, Berlin, 1978.
[6] S.M. Meyers et al., J. Nucl. Mater. 165 (1989) 9.
[7] G. Federici, ITER Joint Central Team; see also ITER Project, Detailed Design Document, IDoMS# G 16 DDD 2 96-11-27 W 0.2, 1996.
[8] F. Waelbroeck et al., Report Jül-1966, Kernforschungsanlage Jülich GmbH, Institut für Plasmaphysik, Association Euratom-KfA, 1984.
[9] M.I. Baskes, J. Nucl. Mater. 92 (1980) 318.
[10] G. Federici et al., Fus. Eng. Des. 39&40 (1998) 445.
[11] M.C. Billone et al., Fus. Eng. Des. 27 (1995) 179.
[12] A.M. Khomutov et al., J. Nucl. Mater. 233–237 (1996) 111.
[13] G.R. Longhurst et al., J. Nucl. Mater. 258–263 (1998) 640.
[14] R.A. Langley, J. Nucl. Mater. 85&86 (1979) 1123.
[15] K. Ashida et al., J. Nucl. Mater. 241–243 (1997) 1060.
[16] M. Mayer, J. Nucl. Mater. 240 (1997) 164.
[17] A.A. Haasz, J.W. Davis, J. Nucl. Mater. 241–243 (1997) 1076.
[18] W.R. Wampler, J. Nucl. Mater. 122/123 (1984) 1598.
[19] W.R. Wampler, unpublished data received in March, 1997.
[20] V.N. Chernikov et al., J. Nucl. Mater. 233–237 (1996) 860.
[21] V. Kh. Alimov, unpublished data, 1997.
[22] R.A. Anderl, unpublished data, 1997.
[23] W. Moller et al., Max-Planck-Institut für Plasmaphysik, IPP-JET Report No. 26, 1985.
[24] R.A. Causey et al., J. Nucl. Mater. 241–243 (1997) 1041.
[25] R.A. Causey, D. Walsh, J. Nucl. Mater. 254 (1998) 84.
[26] R.P. Doerner et al., J. Nucl. Mater., accepted for publication.
[27] R. Doerner et al., in: 17th IEE/NPSS Symposium on Fusion Engineering, San Diego, CA, 6–9 October 1997.
[28] W.R. Wampler et al., J. Nucl. Mater. 233–237 (1996) 791.
[29] H.D. Falter et al., JET unpublished data.
[30] W. Eckstein, Computer Simulation of Ion–Solid Interactions, Springer Series in Materials Science 10, Springer, Berlin, 1991.
[31] N. Yoshida et al., J. Nucl. Mater. 233–237 (1996) 874.
[32] J.M. Beeston et al., EGG-FSP-9215, Idaho National Engineering and Environmental Laboratory, 1990.
[33] W.R, Wampler, J. Nucl. Mater. 196–198 (1992) 981.
[34] M.I. Guseva et al., J. Nucl. Mater. 233–237 (1996) 682.
[35] R.A. Anderl et al., J. Nucl. Mater. 196–198 (1992) 986.
[36] J. Roth et al., J. Nucl. Mater. 250 (1997) 23.
[37] R.A. Anderl et al., J. Fus. Energy 16 (1/2) (1997) 95.
[38] K. Ashida, K. Watanabe, in: Proceedings of the 3rd IEA Int'l Workshop on Beryllium Technology for Fusion, Sangyo Kaikan, Mito City, Japan, 22–24 October 1997, JAERI Conf. 98-001, Janaury 1998.
[39] K. Ashida, K. Watanabe, Fus. Eng. Des. 37 (1997) 307.
[40] J. Won et al., J. Nucl. Mater. 241–243 (1997) 1110.
[41] R.W. Conn et al., Fus. Engr. Des. 37 (1997) 481.

[42] R.A. Causey et al., in: Proceedings of the International Tritium Workshop on Present Status and Prospect of Tritium–Material Interaction Studies, Toyama, Japan, 1996, p. 1.
[43] J.N. Brooks, R. Causey, G. Federici, D. Ruzic, J. Nucl. Mater. 241–243 (1997) 294.
[44] M. Mayer et al., J. Nucl. Mater. 230 (1996) 67.
[45] V. Kh. Alimov, et al., in: Proceedings of the Fourth International Workshop on Tritium Effects in Plasma-Facing Components, Santa Fe, NM, 14–15, May 1998.
[46] M.I. Baskes, SAND83-8231, Sandia National Laboratories, 1983.
[47] H. Verbeek, W. Eckstein, in: S.T. Picraux, E.P. EerNisse, V.L. Vook (Eds.), Application of Ion Beams to Metals, Plenum Press, New York, 1974, p. 597.
[48] M.B. Liu et al., J. Nucl. Mater. 79 (1979) 267.
[49] H. Kawamura et al., J. Nucl. Mater. 176&177 (1990) 661.
[50] R.A. Anderl, ITER US Home Team Report ITER/94/US/TE/SA-21 (12 October 1994) Idaho National Engineering and Environmental Laboratory.
[51] R.A. Anderl et al., in: A.W. Thompson, N.R. Moody (Eds.), Proceedings of the Fifth International Conf. on the Effects of Hydrogen on the Behavior of Materials, Jackson Lake Lodge, Moran, WY, September 11–14, 1994, Hydrogen Effects in Materials, TMS Publications, 1996, p. 105.
[52] K. Touche, B. Terreault, Mater. Res. Soc. Symp. Proc. 316 (1994) 987.
[53] C.B.A. Forty et al., Handbook of Fusion Activation Data, Part 1: Elements Hydrogen to Zirconium, AEA FUS 180, AEA Fusion, Culham Laboratory, Abingdon, Oxon, OX14 3DB, UK, May 1992.
[54] G.R. Longhurst, ITER US Home Team Report ITER/US/97/TE/SA-22 Rev. 1, Idaho National Engineering and Environmental Laboratory, 24 September 1997.
[55] R.A. Anderl et al., Fus. Technol. 28 (1995) 1114.
[56] D.L. Baldwin et al., J. Nucl. Mater. 179–181 (1991) 329.
[57] D.L. Baldwin, M C. Billone, J. Nucl. Mater. 212–215 (1994) 948.
[58] R.A. Anderl et al., in: Proceedings of the Third IEA International Conference on Beryllium Technology for Fusion, 22–24 October 1997, Mito City, Japan, JAERI-Conf. 98-001, 1998.
[59] E. Abramov et al., J. Nucl. Mater. 175 (1990) 90.
[60] F. Scaffidi-Argentina et al., Fus. Technol. 32 (1997) 179.
[61] F. Scaffidi-Argentina et al., Fus. Technol. 33 (1998) 146.
[62] G.R. Longhurst et al., EGG-FSP-10315 (12 June 1992) Idaho National Engineering and Environmental Laboratory.
[63] W. Möller, IPP 9/44, Max Planck Institut für Plasmaphysik, Garching, Germany, 1983.
[64] S. Cho et al., J. Nucl. Mater. 212–215 (1994) 961.
[65] M. Dalle Donne et al., J. Nucl. Mater. 212–215 (1994) 954.
[66] V.I. Shapovalov, Yu.M. Dukel'ski, Russian Metallurgy 5 (1984) 210.
[67] W.L. Hsu et al., J. Nucl. Mater. 176&177 (1990) 218.
[68] P.L. Andrew et al., J. Nucl. Mater. 196–198 (1992) 997.
[69] R.A. Causey, K.L. Wilson, J. Nucl. Mater. 212–215 (1994) 1436.
[70] G. Federici et al., in: 16th IEEE/NPSS Symposium on Fusion Engineering, Urbana, Illinois, 30 September–5 October 1995.
[71] G. Federici, D.F. Holland, ITER Internal Report, 18 January 1996.
[72] G.A. Henshall et al., UCRL-ID-120258, Lawrence Livermore National Laboratory, 1 March 1995.
[73] Unpublished INEEL experimental data.
[74] R.G. Macaulay-Newcombe et al., J. Nucl. Mater. 191–194 (1992) 263.
[75] G. Saibene et al., J. Nucl. Mater. 176&177 (1990) 618.
[76] R. Doerner, University of California, San Diego, and W.R. Wampler, Sandia National Laboratories, Albuquerque, NM, private communication.
[77] G. Federici et al., J. Nucl. Mater. 266–269 (1999) 14.
[78] J.N. Brooks et al., J. Nucl. Mater. 266–269 (1999) 58.